uOttawa

L'Université canadienne
Canada's university

FACULTÉ DES ÉTUDES SUPÉRIEURES ET POSTOCTORALES

uOttawa

L'Université canadienne
Canada's university

FACULTY OF GRADUATE AND POSDOCTORAL STUDIES

Nazish Irfan

AUTEUR DE LA THÈSE / AUTHOR OF THESIS

M.A.Sc. (Electrical Engineering)

GRADE / DEGREE

School of Information Technology and Engineering

FACULTÉ, ÉCOLE, DÉPARTEMENT / FACULTY, SCHOOL, DEPARTMENT

Simulation of Incident Field Coupling with Nonuniform Transmission Lines

TITRE DE LA THÈSE / TITLE OF THESIS

E. Gad

DIRECTEUR (DIRECTRICE) DE LA THÈSE / THESIS SUPERVISOR

CO-DIRECTEUR (CO-DIRECTRICE) DE LA THÈSE / THESIS CO-SUPERVISOR

EXAMINATEURS (EXAMINATRICES) DE LA THÈSE / THESIS EXAMINERS

R. Achar

M. Yagoub

Gary W. Slater

Le Doyen de la Faculté des études supérieures et postdoctorales / Dean of the Faculty of Graduate and Postdoctoral Studies

SIMULATION OF INCIDENT FIELD COUPLING WITH NONUNIFORM TRANSMISSION LINES

by

Nazish Irfan

Thesis submitted to the
Faculty of Graduate and Postdoctoral Studies
In partial fulfillment of the requirements
For the M.A.Sc. degree in
Electrical Engineering

School of Information Technology and Engineering
Faculty of Engineering
University of Ottawa

Your file Votre référence
ISBN: 978-0-494-49213-0
Our file Notre référence
ISBN: 978-0-494-49213-0

Abstract

This thesis develops a new algorithm to simulate incident field coupling with high-speed interconnects. The interconnects considered in this thesis are represented by nonuniform multi-conductor transmission lines and are described through the Telegraphers Equations. The developed algorithm is based on the concept of model-order reduction via projection onto Hilbert space, where a reduced-order model representing the transmission line is constructed and employed as a stamp for representing the line. The incident field is represented by a set of terminal sources obtained from the projection operator used in constructing the reduced-order model. In addition to being developed to handle nonuniform transmission lines, the proposed algorithm offers an advantage by guaranteeing the passivity of the reduced order model. Several examples are presented to validate the validity and accuracy of the proposed algorithm.

Acknowledgements

I would like to express my gratitude and appreciation to my mentor Professor Emad Gad for his able guidance, endless support, kindness and much needed encouragement. His friendly manner, patience, good judgment, motivation in difficult times and strong leadership quality have made this thesis work an enjoyable and memorable experience. I feel privileged to have him as my thesis supervisor.

I would like to acknowledge and thanks several of my friends Mohammad Suruz Mia, Ali Amine, Gurpreet Singh Shinh, Ben, Sreejit Nair and Shafiq for useful discussions and for their help when I needed. I would also like to express my gratitude to students, professors and staff at department of electrical engineering for making my work at Ottawa University a memorable experience.

My final thoughts are with my parents, Abdul Mobin and Saida Begum, my brother Tauseef and sisters Farzana and Ateeya, my wife Nafisa and my son Inayat. Without their patience, encouragement and backing working on this thesis would be impossible. I am grateful to all.

Abbreviations

BC	Boundary Conditions
UMTL	Uniform Multi-conduct
BVPs	Boundary Value Problems
EMI	Electromagnetic Interference
ICs	Initial Condition
ICT	Integrated Congruence Transform
IFFT	Inverse Fast Fourier Transform
IFC	Incident Field Coupling
IVP	Initial Value Problem
MGS	Modified-Gram Schmidth
MNA	Modified Nodal Analysis
MoC	Method of Characteristic
MRA	Matrix-Rational Approximation
MTL	Multi-conductor Transmission Lines
NMTL	Non-Uniform Multi-conductor Transmission Line
ODEs	Ordinary Differential Equations
PCB	Printed Circuit Board
PDEs	Partial Differential Equations
PUL	Per-unit Length
Q-TEM	quasi-Transverse Electromagnetic Mode
STM	State Transition Matrix
TDSE	Time Domain Space Expansion
TEM	Transverse Electro Magnetic
TEs	Telegrapher's Equation
VLSI	Very Large Scale Integration

Contents

List of Figures

Chapter 1

Introduction

1.1 Background and Motivation

Rapid advancement in VLSI (Very Large Scale Integration) and wireless industry toward higher operating frequencies, miniature designs and increased integration of mixed analog/digital systems is making the signal integrity analysis a challenging task. Operating at high frequency has highlighted effects such as signal distortion, dispersion, delay, crosstalk, electromagnetic radiation and interference, which are giving major challenges in the design of high-speed electrical systems [1], [2]. These effects if not considered properly during the design stage can effect the functional performance of the system as well as may lead to permanent hardware failure. Considering this effect timely would significantly reduce post-production corrections, time to market, reduce cost and would result in more reliable product.

Interconnects can exist at all levels of design hierarchy such as on-chip, packaging structures, multi chip modules, printed circuit boards and backplanes. At high frequencies, a simple wire interconnect cannot be treated as a short-circuit as it behaves as a distributed structure. Moreover these distributed structures have to be incorporated along with other circuit components in general circuit simulator. Hence a reliable prediction of their behavior and its effect on system performance requires proper modeling and efficient analysis tools.

One of the major challenges that arise in designing systems with high speed interconnects is the susceptibility to electromagnetic interference (EMI). EMI can severely degrade the signal integrity of the system. The basic mechanism for EMI occurs as a result of the coupling between the incident electromagnetic field and the electrical

interconnect which typically functions as an antenna [3], [4], [5].

Modeling of high-speed interconnects is usually done with various levels of complexity that could range from simple RC Ladder networks to full-wave 3D models derived from Maxwell's equation [1], [6], [7], depending on the operating frequency and the size of the interconnects. However, when the interconnect becomes electrically long at the highest operating frequency, a Transverse Electromagnetic Mode (TEM) becomes the dominant mode of propagation along the interconnect. Under the Quasi TEM operation, interconnects are modeled as lossy coupled Multi-conductor Transmission Lines (MTL) with per-unit-length parameter matrices which could be frequency dependent to capture the peculiar high frequency phenomena such as proximity and edge effects [2].

In fact, MTLs are represented by the Telegrapher's Equations (TEs) which are partial differential equations (PDEs) that involve the time dimension and a single spatial dimension representing the longitudinal dimension along which the signal propagates.

The objective of estimating EMI effects on high-speed interconnects has been mainly approached by treating the interconnects as MTL, while representing the incident field by a distributed source added to the TE as a forcing term.

Nonetheless, the main bottleneck in including the TE with general circuit simulators remained in the fact that they are PDEs that involve a spatial dimension in addition to the time domain. Although the TE can be converted into a set of ordinary differential equations (ODEs) via the Laplace transformation, there is a little value to be harvested from having such a pure frequency-domain description, given that general circuits contain nonlinear elements which can be only represented through the time-domain. The problem of incorporating the TE in general circuit simulators is known as the mixed frequency-time problem and has been described extensively in [1].

Several approaches have appeared in the literature to handle the mixed frequency-time problem in the context of simulating the incident field coupling with MTLs. In general accurate analysis of circuits having interconnects under external field necessitates incorporating field coupling equations with conventional circuit formulation techniques such as Modified Nodal Analysis (MNA). For this purpose, SPICE models were proposed for the field coupling to lossless transmission lines [8], [9], [10] based on method of characteristics [11], [12] and model-order reduction approaches [13] based on asymptotic waveform evaluation [14]. Also, lossy MTLs were handled in [15] by discretizing the distributed sources along the lines (which quickly becomes inefficient for long lines), based on method of characteristics [16], and in [5] based on multi point expansion technique and complex frequency hopping [6].

However one of the major difficulties with the above methods is that they do not guarantee the passivity of the MTL macromodel. Passivity is an important property because stable but nonpassive models may lead to unstable transient simulations. Passive matrix-rational approximation (MRA) [17], [18] based on closed-form MTL macromodel was suggested for field coupling analysis in [3] and was extended to efficiently handle low loss interconnects [19].

Nevertheless, MRA based techniques have been developed based on the exponential matrix which is valid only for uniform MTL (UMTL) in which the per-unit length parameter matrices are independent of the spatial variables of the TE. Nonuniform MTL (NMTL), on the other hand, represent an important segment of interconnect structures in which the per-unit-length parameter matrices are functions of the spatial variable in the TE. Unfortunately the MRA technique can not handle the case of NMTL since the corresponding TE cannot be solved analytically using the matrix exponential.

1.2 Objective of the Thesis

The main objective of this thesis is to develop a passivity-preserving algorithm to simulate electromagnetic field coupling with circuits having high speed interconnects that are modeled as NMTL. The developed algorithm should be equipped to handle NMTL while at the same time be valid to treat UMTL as a special case.

To achieve these objectives, this thesis will investigate the idea of using the concept of Integrated Congruence Transform (ICT) in developing the macromodel and the equivalent sources representing the incident electromagnetic field. It is to be noted that the ICT algorithm was first introduced in [20] and later extended in [21] to handle the NMTL simulation but with no EMI. The work presented in this thesis seeks to generalize the ICT framework in order to address the problem of incident field coupling.

1.3 Contribution

The basic contribution of this thesis is the demonstration that the theoretical framework of the ICT algorithm can be carried and extended to simulate the incident field coupling with NMTLs, while providing a guarantee of passivity for the macromodel used in the simulation. The thesis presents an algorithm for using the ICT to derive a macromodel for NMTL as well as equivalent sources representing the incident field that is suitable for

circuit simulators. The proposed algorithm has been validated by comparing the results obtained to the results obtained from the analytical solutions available for special cases of NMTL. Good agreement between both results have been observed and reported in the thesis.

1.4 Organization of Thesis

Chapter-2 presents a brief introduction to the transmission line theory and derives a compact form of the TEs that includes the incident electromagnetic field. Chapter-3 discusses the simulation techniques used to simulate the case of incident field coupling to transmission line. Chapter-4 discusses the fundamental theory of Integrated Congruence Transform, and presents a new algorithm to employ this theory to simulate the incident field coupling with nonuniform transmission lines. Chapter-5 presents the numerical examples and Chapter-6 presents the conclusion and suggestions for the further research.

Chapter 2

Formulation of Interconnects

Depending upon the desired accuracy and the operating frequency, different interconnect models may be necessary and each model presents different challenges for simulation. In this chapter we will briefly discuss different interconnect models. We will also discuss the derivation of inhomogeneous Telegrapher's equations describing the quasi-TEM distributed models of interconnects exposed to EMI.

2.1 Interconnect Models

Generally the modeling approach used in modeling high speed interconnects can be classified as either one that is based on simple realization using lumped network, or one that is based on distributed models. While the lumped model uses a heuristic way to capture mainly the effect of the interconnect using simple RC circuit, the distributed model is derived from the basic principles of electromagnetic theory using Maxwell's Equations. It should be noted, however, that the realization of a distributed model can be accomplished via a network of lumped components, which should be clearly distinguished from a lumped network not based on the Electromagnetic Theory.

2.1.1 Lumped Models

At low operating frequency, interconnect could be modeled using RC or RLC circuit models. RC tree model is RC circuits with capacitors from all nodes to ground (no floating capacitors and no resistors to ground). RC circuits response are monotonic in nature. The signal delay through RC circuit is often estimated by using Elmore delay [7] model. Typically RC circuit is a low pass filter, therefore RC model is not an accurate model if

we wish to incorporate the high frequency issues like cross talk and ringing. This model implies that the high frequency components of the current flowing in the interconnect return through the capacitors and also does not say anything about the return path of dc or low frequency components of the current. With this assumption, it is difficult to model inductance, which is defined by the closed loop. Therefore, RLC model [22] can be used for estimating inductive effect such as delay, overshoot etc. The response of the RLC circuits may be non-monotonic. A single time constant approximation with Elmore delay is not generally sufficient for such circuits. Two time-constant models have been shown to improve the accuracy, but only as compared to RC tree monotone response approximations [23]. Usually lumped interconnect circuits extracted from layout contains a large number of nodes that make the simulation highly CPU intensive. Figure 2.1 shows general lumped interconnect model, where L is the inductance, R is the resistance, G is the conductance and C is the capacitance of the interconnect.

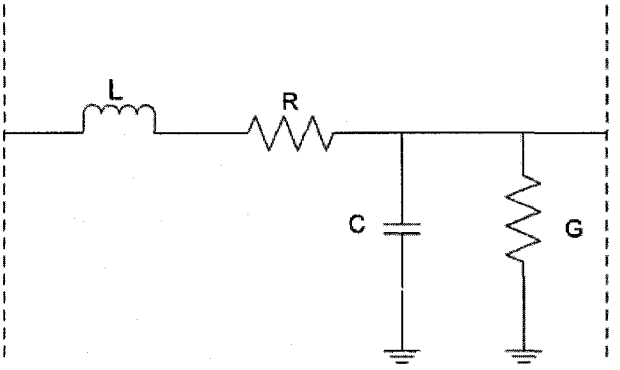

Figure 2.1: Lumped Transmission Line Model

2.1.2 Distributed Models

When the interconnect length becomes electrically large, i.e., the structures largest dimension (length) is much larger than the shortest operating wavelength then the conventional lumped model cannot be used and we have to use distributed models derived from the electromagnetic theory using Maxwell's Equations.

One of the basic assumptions that can be made about the propagation of electromagnetic field over interconnects is that it satisfies a Transverse Electromagnetic Mode (TEM) in which both of the electric and magnetic field are perpendicular to each other and to the direction of propagation.

With this assumption, Maxwell's Equations can be shown to reduce to a set of coupled partial differential equations known as the Telegraphers Equations (TEs). A convenient advantage of these equations is that they model the interconnect in terms of voltages and currents rather that in classical electromagnetic quantities, which is more appropriate in the context of circuit simulators.

It should be noted, however, that other higher operating modes may exist in addition to the TEM modes. For example, having electrically large cross-sectional dimensions or using imperfect conductors may violate the TEM mode assumption. Moreover, operating at high frequency gives rise to the skin edge and proximity effects which in turn violate the stand-along TEM mode propagation underlying the TEs.

Nonetheless such effects can be incorporated by using the so-called quasi-TEM (Q-TEM) in which the TEs are modified by using a resistance per-unit-length parameters matrix to account for the losses in the interconnect conductors and by allowing the per-unit-length matrices to be frequency-dependent to account for the high-speed effects such as skin, depth and edge and proximity effects.

Derivation of the TEs from Maxwell's equations can be found in [2]. Given that the main focus of this thesis is on the effect of incident field on interconnects the following section will present the derivation of TEs with the presence of incident electromagnetic field.

2.2 Derivation of Telegrapher's Equations with Incident Field Coupling

The incident field on the multiconductor transmission lines may be in the form of uniform plane waves such as those generated by distant transmitting antennas or they may be non-uniform fields such as those generated by a nearby radiating structure. We can incorporate the effect of incident EMI field on the multiconductor transmission line as a distributed source along the lines [2].

The effect of incident EMI field on the transmission line was first considered for two-conductor lines in [24], [25]. This was later extended to multiconductor lines in [15]. The assumption of quasi-TEM mode is valid if the conductor length is much smaller than the wavelength of interest and conductor losses and effect due to inhomogeneity of the dielectric media are small.

In this section, we will derive TEs for the multiconductor transmission lines in the

presence of incident field. The derivations presented here are based on the presentation given in [26].

2.2.1 Derivation of first Telegrapher's equation with IFC

Consider an $(n+1)$ conductor uniform transmission line as shown Figure 2.2. Applying Maxwell-Faraday law [27] over the rectangular area S_i enclosed by contour C_i we get

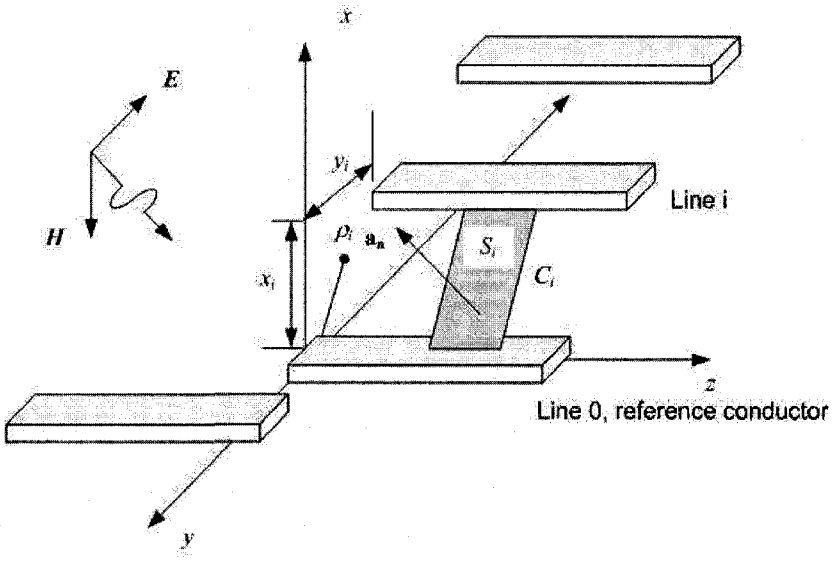

Figure 2.2: Interconnect excited by arbitrary incident field

$$\oint_{C_i} \vec{E}.\vec{dl} = -s \oint_{S_i} \vec{B}.\vec{dS} \tag{2.1}$$

where $\vec{E}$ and $\vec{B}$ are the phasors of the total electric and magnetic fields, s is the complex frequency and subscript i stands for the i^{th} conductor. Expanding the integral in LHS of (2.1) and separating the magnetic field $\vec{B}$ into its incident and scattered components $\vec{B}^{\text{inc}}$ and $\vec{B}^{\text{sct}}$, respectively, we get

$$\int_{\rho(x_i,y_i)} \vec{E}_\rho(\rho, z+\Delta z)\vec{d\rho} - \int_z^{z+\Delta z} \vec{E}_z(\rho_i, z)\vec{dz} - \int_{\rho(x_i,y_i)} \vec{E}_\rho(\rho, z)\vec{d\rho} + \int_z^{z+\Delta z} \vec{E}_z(\rho_0, z)\vec{dz} = -s\int_{S_i} \vec{B}^{inc}.\vec{dS} - s\int_{S_i} \vec{B}^{\text{sct}}.\vec{dS} \tag{2.2}$$

where $\vec{E}_\rho(\rho, z)$ and $\vec{E}_z(\rho_i, z)$ are respectively, the components of the electric field in the transverse plane and the z-direction and ρ is a parameter that defines points in the transverse plane. Since the structure supports Quasi TEM mode of propagation, the transverse fields are of static nature. Hence the voltage between any point in the transverse plane can be written as

$$\begin{aligned} V_i(z) &= -\int_{\rho(x_i,y_i)} \vec{E}_\rho(\rho, z)\vec{d\rho} \\ V_i(z+\Delta z) &= -\int_{\rho(x_i,y_i)} \vec{E}_\rho(\rho, z+\Delta z)\vec{d\rho} \end{aligned} \tag{2.3}$$

Since the magnetic filed is of the transverse nature, the scattered magnetic field can be

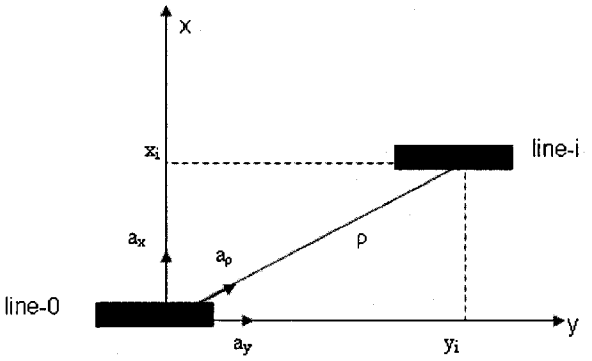

Figure 2.3: Transverse plane parameters of the MTL system

related to the currents via the per-unit length inductances (L_i, i^{th} conductor) as

$$\lim_{\Delta z \to o} \frac{1}{\Delta z} \int_{Si} \vec{B}^{\text{sct}}.\vec{dS} = -\sum_{k=1}^{n} L_{ik} I_k(z) \tag{2.4}$$

Let us represent the imperfect conductors with per-unit-length resistances, R_i. The total longitudinal fields are related to the currents on the conductors are as follows

$$\begin{aligned} \int_z^{z+\Delta z} \vec{E}_z(\rho_i, z)\vec{dz} &= R_i \Delta z I_i(z) \\ -\int_z^{z+\Delta z} \vec{E}_z(\rho_o, z)\vec{dz} &= R_o \Delta z \sum_{k=1}^{n} I_k(z) \end{aligned} \tag{2.5}$$

The current in the signal conductor is assumed to be equal to, and opposite in direction to the current in the reference conductor. This is equivalent to considering differential mode current and neglecting common mode currents. Neglecting common mode current is valid assumption since we are interested in the final results at the termination where only differential mode current flows. Substituting (2.3)-(2.5) in (2.2) we get

$$-V_i(z+\Delta z)+V_i(z)-R_i\Delta z I_i(z)-R_o\Delta z\sum_{k=1}^{n} I_k(z) = s\Delta z\sum_{k=1}^{n} L_{ik}I_k(z)-s\int_{Si}\vec{B}^{\text{inc}}.\vec{dS} \quad (2.6)$$

Dividing (2.6) by Δz, taking the limit $\Delta z \rightarrow 0$, and expressing in matrix form we get

$$\frac{d}{dz}\boldsymbol{V}(z) + (\boldsymbol{R}+s\boldsymbol{L})\boldsymbol{I}(z) = \begin{bmatrix} \vdots \\ s\int_{\rho(x_i,y_i)} \vec{B}_n^{\text{inc}}\vec{d\rho} \\ \vdots \end{bmatrix} \quad (2.7)$$

We see that the RHS of (2.7) depends on the incident magnetic field. The forcing function in RHS of (2.7) can be more conveniently expressed in terms of only the incident electric fields by using Faraday's law around the contour C_i in terms of incident fields alone,

$$\int_{\rho(x_i,y_i)} \vec{E}_\rho^{\text{inc}}(\rho, z+\Delta z)\vec{d\rho} - \int_z^{z+\Delta z} \vec{E}_z^{\text{inc}}(\rho_i, z)\vec{dz} - \int_{\rho(x_i,y_i)} \vec{E}_\rho^{\text{inc}}(\rho, z)\vec{d\rho} + \int_z^{z+\Delta z} \vec{E}_z^{\text{inc}}(\rho_o, z)\vec{dz} = -s\int_{S_i}\vec{B}^{\text{inc}}.\vec{dS} \quad (2.8)$$

Dividing (2.8) by Δz, taking the limit $\Delta z \rightarrow 0$

$$s\int_{\rho(x_i,y_i)} \vec{B}_n^{\text{inc}}\vec{d\rho} = -\frac{d}{dz}\int_{\rho(x_i,y_i)} \vec{E}_\rho^{\text{inc}}(\rho, z)\vec{d\rho} + E_\rho^{\text{inc}}(\rho_i, z) - E_\rho^{\text{inc}}(\rho_o, z) \quad (2.9)$$

Substituting (2.9) in (2.7), we obtain the first set of inhomogeneous TE's as

$$\frac{d}{dz}\boldsymbol{V}(z)+(\boldsymbol{R}+s\boldsymbol{L})\boldsymbol{I}(z) = \begin{bmatrix} \vdots \\ -\frac{d}{dz}\int_{\rho(x_i,y_i)} \vec{E}_\rho^{\text{inc}}(\rho, z)\vec{d\rho} + E_\rho^{\text{inc}}(\rho_i, z) - E_\rho^{\text{inc}}(\rho_o, z) \\ \vdots \end{bmatrix} \quad (2.10)$$

2.2.2 Derivation of second TEs with IFC

The second MTL equation can be derived by enclosing the i^{th} conductor with a closed surface as in Figure 2.4 and applying the continuity equation

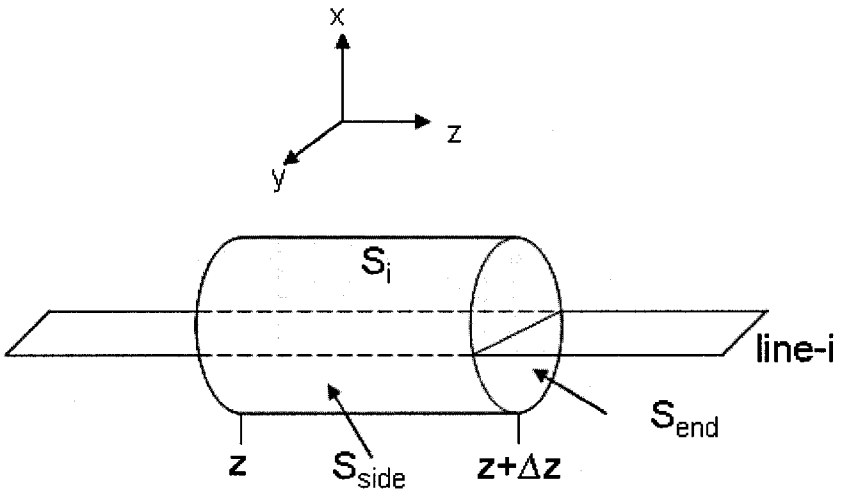

Figure 2.4: Defining Surface for MTL equation

$$\oint_{S_i} \vec{J}.d\vec{S} = -sQ_{\text{enc}} \tag{2.11}$$

Over the end caps, i.e, at the S_{end}, we have

$$\int_{S_{\text{end}}} \vec{J}.d\vec{S} = I_i(z+\Delta z) - I_i(z) \tag{2.12}$$

Over the sides of the surface, i.e, at the S_{side}, we have

$$\int_{S_{\text{side}}} \vec{J}.d\vec{S} = \sigma \int_{S_{\text{side}}} \vec{E}_{\rho}^{\text{sct}}.d\vec{S} \tag{2.13}$$

Here, $\vec{E}_{\rho}^{\text{sct}}$ represents the transverse component of the scattered electric field and σ, ϵ are the conductivity and permittivity of the surrounding homogeneous medium, respectively.

Now we define the per-unit-length conductance and capacitance matrices as

$$s \lim_{\Delta z \to o} \frac{1}{\Delta z} \int_{S_{\text{side}}} \vec{B}^{\text{sct}}.d\vec{S} = \left[-G_{i1} \cdots \sum_{k=1}^{n} G_{ik} \cdots - G_{in} \right] \begin{bmatrix} V_1^{\text{sct}}(z) \\ \vdots \\ V_i^{\text{sct}}(z) \\ \vdots \\ V_n^{\text{sct}}(z) \end{bmatrix} \tag{2.14}$$

$$\epsilon \lim_{\Delta z \to o} \frac{1}{\Delta z} \int_{S_{\text{side}}} \vec{B}^{\text{sct}}.d\vec{S} = \left[-C_{i1} \cdots \sum_{k=1}^{n} C_{ik} \cdots - C_{in} \right] \begin{bmatrix} V_1^{\text{sct}}(z) \\ \vdots \\ V_i^{\text{sct}}(z) \\ \vdots \\ V_n^{sct}(z) \end{bmatrix} \tag{2.15}$$

By Gauss's Law [27] we have

$$Q_{\text{enc}} = \epsilon \int_{S_{\text{side}}} \vec{E}_{\rho}^{\text{sct}}.d\vec{S} \tag{2.16}$$

Now substituting (2.12), (2.13), (2.15) into (2.11), and dividing both side by Δz and taking limit as $\Delta z \to 0$ we get

$$\frac{d}{dz}\boldsymbol{I}(z) + (\boldsymbol{G} + s\boldsymbol{C})\boldsymbol{V}^{\text{sct}}(z) = 0 \tag{2.17}$$

We can write the same equation in total voltage form as

$$\boldsymbol{V}(z) = \boldsymbol{V}^{\text{sct}}(z) - \int_{\rho(x,y)} \vec{E}_{\rho}^{\text{inc}}(\rho, z)\vec{d}\rho \tag{2.18}$$

Substituting (2.18) into (2.17) gives the second set of inhomogeneous Telegrapher's equation

$$\frac{d}{dz}\boldsymbol{I}(z) + (\boldsymbol{G} + s\boldsymbol{C})\boldsymbol{V}(z) = -(\boldsymbol{G} + s\boldsymbol{C}) \begin{bmatrix} \vdots \\ \int_{\rho(x_i,y_i)} \vec{E}_{\rho}^{inc}(\rho, z)\vec{d}\rho \\ \vdots \end{bmatrix} \tag{2.19}$$

2.3 Compact Form of Telegrapher's Equation with Incident Field Coupling

We have derived the two fundamental equations for TEs in the above section. Now we will write them in compact form. We can write(2.10) and (2.19) as

$$\frac{d}{dz}\begin{bmatrix} \boldsymbol{V}(z,s) \\ \boldsymbol{I}(z,s) \end{bmatrix} = \boldsymbol{Q}(s)\begin{bmatrix} \boldsymbol{V}(z,s) \\ \boldsymbol{I}(z,s) \end{bmatrix} + \hat{\boldsymbol{F}}(z,s) \tag{2.20}$$

where

$$\boldsymbol{Q}(s) = \begin{bmatrix} \boldsymbol{0} & -\boldsymbol{R} \\ -\boldsymbol{G} & \boldsymbol{0} \end{bmatrix} + s\begin{bmatrix} \boldsymbol{0} & -\boldsymbol{L} \\ -\boldsymbol{C} & \boldsymbol{0} \end{bmatrix} \tag{2.21}$$

The distributed source due to incident fields in (2.10) and (2.19) is represented by $\widehat{\mathbf{F}}(z,s)$ in (2.20), and is given by

$$\widehat{\mathbf{F}}(z,s) = \begin{bmatrix} \boldsymbol{V}_d(z,s) \\ \boldsymbol{I}_d(z,s) \end{bmatrix} = \begin{bmatrix} \frac{d}{dz}\boldsymbol{V}_t^{\text{inc}}(z,s) + \boldsymbol{V}_z^{\text{inc}}(z,s) \\ (\boldsymbol{G}+s\boldsymbol{C})\boldsymbol{V}_t^{\text{inc}}(z,s) \end{bmatrix} \tag{2.22}$$

where

$$\begin{aligned} \boldsymbol{V}_t^{inc}(z,s) &= \begin{bmatrix} \vdots \\ \int_{\rho_{(x,y)}} \vec{E}_\rho^{\text{inc}}(\rho_{(x,y)},z)d\rho \\ \vdots \end{bmatrix} \\ \boldsymbol{V}_z^{\text{inc}}(z,s) &= \begin{bmatrix} \vdots \\ E_z^{\text{inc}}(x_i,y_i,z) - E_z^{\text{inc}}(x_0,y_0,z) \\ \vdots \end{bmatrix} \end{aligned} \tag{2.23}$$

2.3.1 Distributed Sources due to Incident Plane Wave

For most practical cases, the wavelength of the incident field is small compared to the distance between the interferer and tested system. Therefore, in such cases the analyzed transmission lines are situated in the far field of the spherical incident field, which could locally be approximated by uniform plane wave [2]. In this case, the electric field of the

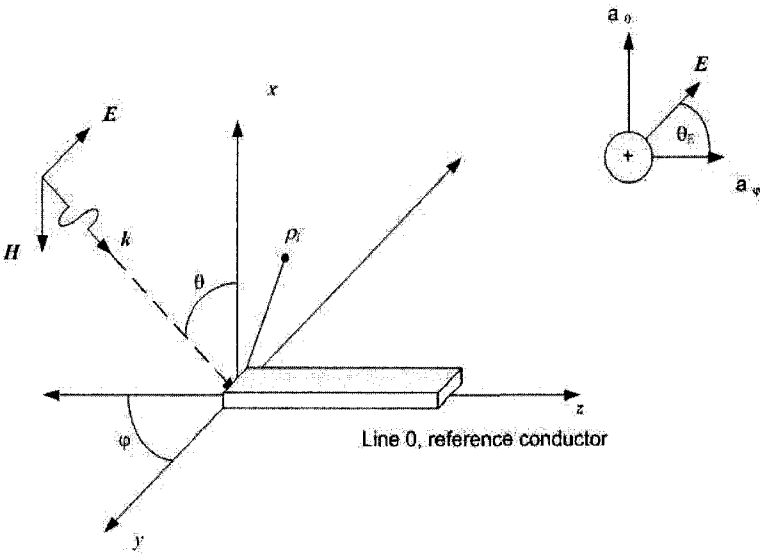

Figure 2.5: Incident Field Parameter

incident uniform plane wave can be represented in the frequency domain as [28]

$$\vec{E}(x,y,z) = E_0(s)(A_x\widehat{a}_x + A_y\widehat{a}_y + A_z\widehat{a}_z)e^{-s(k_x x + k_y y + k_z z)} \tag{2.24}$$

where $E_0(s)$ is the complex amplitude of the plane wave and A_x, A_y and A_z are the components of the incoming uniform plane wave along x, y and z axes of rectangular coordinate system respectively.

The components of the electric field can be defined in terms of the direction cosines as follows. We can define direction cosines of the electric field vector as

$$\begin{aligned} A_x &= \sin\theta_E \sin\theta \\ A_y &= -\sin\theta_E \cos\theta\cos\phi - \cos\theta_E \sin\phi \\ A_z &= -\sin\theta_E \cos\theta\sin\phi + \cos\theta_E \cos\phi \\ k_x &= \frac{-\cos\theta}{c} \\ k_y &= \frac{-\sin\theta\cos\phi}{c} \\ k_z &= \frac{\sin\theta\sin\phi}{c} \end{aligned} \tag{2.25}$$

where c is the speed of the phase front. Now we can derive closed form formulation

of distributed current and voltage sources by using (2.24) and (2.25) as shown in the following sections.

2.3.2 Simplyfing Distributed Voltage Sources

In this section, we seek to simplify the representation of incident distributed sources in (2.22) and (2.23). The manipulation of these sources carried out in this section has been based upon the derivations presented in [19] and is mainly aimed at facilitating the implementation of the proposed algorithm given in Chapter 4 [2]. From Fig 2.3 we see that

$$\begin{aligned} \frac{x}{\rho} &= \frac{x_i}{d} \\ \frac{y}{\rho} &= \frac{y_i}{d} \\ d &= (x_i + y_i)^{\frac{1}{2}} \end{aligned} \tag{2.26}$$

Now (2.23) can be simplified using the above relation and (2.24)

$$\begin{aligned} V_t^{\text{inc}}(z,s) &= -E_0(s)e^{-sk_z z}\int_0^d \frac{(A_x x_i + A_y y_i)}{d} e^{-s(k_x x_i + k_y y_i)\frac{\rho}{d}} d\rho \\ &= -E_0(s)e^{-sk_z z}\frac{(A_x x_i + A_y y_i)}{s(A_x x_i + A_y y_i)}[1 - e^{-s(k_x x_i + k_y y_i)}] \end{aligned} \tag{2.27}$$

Using the assumption made earlier about the quasi-TEM mode, whereby the cross-sectional dimension of the TL was assumed to be much smaller then the smallest wavelength of interest, we can approximate the exponential term by the first two terms of its Taylor series. This leads to the following

$$\begin{aligned} V_t^{\text{inc}}(z,s) &\approx -E_0(s)e^{-sk_z z}\frac{(A_x x_i + A_y y_i)}{s(k_x x_i + k_y y_i)}[s(k_x x_i + k_y y_i)] \\ &= -E_0(s)e^{-sk_z z}(A_x x_i + A_y y_i) \end{aligned} \tag{2.28}$$

Therefore

$$\frac{d}{dz}V_t^{\text{inc}}(z,s) = sk_z E_0(s)e^{-sk_z z}(A_x x_i + A_y y_i) \tag{2.29}$$

From (2.23) V_z^{inc} can be computed for the i^{th} line using (2.24), where we obtain

$$V_z^{\text{inc}}(z,s) = E_0(s)A_z(e^{-s(k_x x_i + k_y y_i)} - 1)e^{-sk_z z} \tag{2.30}$$

Now approximating the exponential term in (2.30) by its linear Taylor series expansion, we get

$$V_z^{\text{inc}}(z,s) \approx -s(k_x x_i + k_y y_i)E_0(s)A_z e^{-sk_z z} \tag{2.31}$$

Using (2.29) and (2.31) the distributed voltage sources for the i^{th} line can be represented as

$$\begin{aligned} V_d(z,s) &= \frac{d}{dz}V_t^{\text{inc}}(z,s) + V_z^{\text{inc}}(z,s) \\ &= sk_z E_0(s)e^{-sk_z z}(A_x x_i + A_y y_i) - s(k_x x_i + k_y y_i)E_0 A_z e^{-sk_z z} \\ &= sE_0(s)[k_z(A_x x_i + A_y y_i) - A_z(k_x x_i + k_y y_i)]e^{-sk_z z} \end{aligned} \tag{2.32}$$

Let

$$\begin{aligned} \phi_i^{\pm} &= A_x x_i \pm A_y y_i \\ \psi_i^{\pm} &= k_x x_i \pm k_y y_i \end{aligned} \tag{2.33}$$

Distributed voltage source vector can be represented by using (2.33) in a convenient form as

$$\boldsymbol{V}_d(z,s) = sE_0(s)e^{-sk_z z}\tilde{\boldsymbol{v}}_{F1} \tag{2.34}$$

For transmission medium without a solid ground plane, we have

$$\tilde{\boldsymbol{v}}_{F1} = \begin{bmatrix} \vdots \\ k_z\phi_i^+ - A_z\psi_i^+ \\ \vdots \end{bmatrix} \tag{2.35}$$

For a ground plane backed structure (such as a microstrip), it can be proved on similar grounds, using image theory that

$$\tilde{\boldsymbol{v}}_{F1} = \begin{bmatrix} \vdots \\ k_z(\phi_i^+ + \phi_i^-) - A_z(\psi_i^+ - \psi_i^-) \\ \vdots \end{bmatrix} \tag{2.36}$$

2.3.3 Simplyfing Distributed Current Sources

Using (2.28), the distributed current source for the incident field as represented in (2.22) and (2.23) can be written as

$$\begin{aligned} \boldsymbol{I}_d(z,s) &= (\boldsymbol{G}+s\boldsymbol{C}) \begin{bmatrix} \vdots \\ -E_0(s)e^{-sk_z z}(A_x x_i + A_y y_i) \\ \vdots \end{bmatrix} \\ &= E_0(s)e^{-sk_z z}(\boldsymbol{G}+s\boldsymbol{C})\tilde{\boldsymbol{v}}_{F2} \end{aligned} \tag{2.37}$$

For the case of transmission medium without a solid ground plane, we can write as

$$\tilde{\boldsymbol{v}}_{F2} = \begin{bmatrix} \vdots \\ -\phi_i^+ \\ \vdots \end{bmatrix} \tag{2.38}$$

For a ground plane backed structure (such as a microstrip), we can write as

$$\tilde{\boldsymbol{v}}_{F2} = \begin{bmatrix} \vdots \\ -(\phi_i^+ + \phi_i^-) \\ \vdots \end{bmatrix} \tag{2.39}$$

Now the distributed source derived can be written as

$$\begin{aligned} \widetilde{\boldsymbol{F}}(z,s) &= \begin{bmatrix} \boldsymbol{V}_d(z,s) \\ \boldsymbol{I}_d(z,s) \end{bmatrix} \\ &= \widetilde{\Gamma}(s)e^{-sk_z z} \end{aligned} \tag{2.40}$$

Where $\widetilde{\Gamma}(s)$ describes the interaction of the incident field with the lines in the transverse plane and from (2.34) and (2.37) we have

$$\widetilde{\Gamma}(s) = E_0(s) \begin{bmatrix} s\boldsymbol{U}_n & \boldsymbol{0} \\ \boldsymbol{0} & (\boldsymbol{G}+s\boldsymbol{C}) \end{bmatrix} \begin{bmatrix} \tilde{\boldsymbol{v}}_{F1} \\ \tilde{\boldsymbol{v}}_{F2} \end{bmatrix} \tag{2.41}$$

where $\boldsymbol{U}_n$ is a unity matrix of size n. Note that n represents the number of signal conductors in the MTL system.

Therefore the Telegrapher's equation for the incident field coupling represented in (2.20) can be re-written as

$$\frac{d}{dz}\begin{bmatrix} \boldsymbol{V}(z,s) \\ \boldsymbol{I}(z,s) \end{bmatrix} = \boldsymbol{Q}(\boldsymbol{s})\begin{bmatrix} \boldsymbol{V}(z,s) \\ \boldsymbol{I}(z,s) \end{bmatrix} + \widetilde{\Gamma}(s) \tag{2.42}$$

Chapter 3

Simulation Techniques of High Speed Interconnects

This chapter presents a brief background on the main approaches that appeared in the literature to address the problem of simulating the incident field coupling with interconnects modeled as MTLs.

It will be demonstrated that those techniques have been mainly developed for uniform MTL in which the per-unit-length parameters are independent of the spatial variable z of the TEs. Handling the more general case of nonuniform MTL was described in [29], [8] and was approached mainly by dividing the nonuniform line into many sections such that the per-unit-length matrices may be considered constant over the length of each section. With this technique the NMTL can be treated as many cascaded sections of uniform MTL. The main difficulty with this technique lies in the piecewise-constant approximation of the characteristic impedance which causes abrupt reflections at the boundary of each section and can be only minimized if the lengths of the individual sections become infinitesmally small.

Another issue of equal importance in addressing the problem of simulating the incident field coupling with MTL in general is the issue of passivity. This issue typically arises in the macromodeling of the interconnect, where a non-passive mcacromodel can be unstable when terminated with nonlinear components representing the circuit terminations of the interconnect. The issue of passivity will also be highlighted in the course of reviewing the main techniques presented in this chapter.

3.1 Method of Characteristics

The Method of Characteristic (MoC) represents one of the earliest approaches to simulation of transmission line. It was first proposed by Branin [11] to handle lossless transmission lines and has been extended in [12] to address the general case of coupled lossy MTL. The main advantage in MoC-based approaches is that it can handle the delay effect separately from the attenuation effect in MTL [30]. This fact provides a significant speed up in simulating long PCB interconnects which are characterized by small ohmic losses and dominated mainly by delay effect.

Extending MoC-based approaches to simulating incident field coupling with MTL was proposed in [31] and [16]. The basic approaches used there is summarized next. It works by representing the line characteristics in terms of the scattering parameters.

$$\begin{bmatrix} \boldsymbol{B}_1 \\ \boldsymbol{B}_2 \end{bmatrix} = \begin{bmatrix} \boldsymbol{S}_{11} & \boldsymbol{S}_{12} \\ \boldsymbol{S}_{21} & \boldsymbol{S}_{22} \end{bmatrix} \begin{bmatrix} \boldsymbol{A}_1 \\ \boldsymbol{A}_2 \end{bmatrix} \tag{3.1}$$

Where $\boldsymbol{S}_{ij}$ is the scattering parameters, and $\boldsymbol{A}_1$, $\boldsymbol{B}_1$ and $\boldsymbol{A}_2$, $\boldsymbol{B}_2$ represent the incident and reflected current waves at the the two ends of the transmission line.

Incorporating the incident field into the above equation is carried out by using the equivalent sources given by

$$\begin{aligned} \overline{\boldsymbol{B}}_{f1} &= -\frac{1}{2}\int_0^{\mathcal{L}} \boldsymbol{H}(z)\left[\boldsymbol{Y}\overline{\boldsymbol{E}}(s,z) - \overline{\boldsymbol{I}}(s,z)\right] dz \\ \overline{\boldsymbol{B}}_{f2} &= \frac{1}{2}\int_0^{\mathcal{L}} \boldsymbol{H}(\mathcal{L}-z)\left[\boldsymbol{Y}\overline{\boldsymbol{E}}(s,z) + \overline{\boldsymbol{I}}(s,z)\right] dz \end{aligned} \tag{3.2}$$

where

- $\mathcal{L}$ is the transmission line length.
- $\overline{\boldsymbol{B}}_{f1}$, $\overline{\boldsymbol{B}}_{f2}$ represents the equivalent current wave sources accounting for the distributed incident filed.
- $\boldsymbol{E}(s,z)$, $\boldsymbol{I}(s,z)$ are the distributions of series voltage and shunt-current generators included along the line conductors by the external fields,
- $\boldsymbol{H}(z)$ is the matched transmission matrix of current waves
- $\boldsymbol{Y}$ is the characteristic admittance of transmission line given by (3.3).

$$\boldsymbol{Y}(s) = \sqrt{(\boldsymbol{R} + s\boldsymbol{L})^{-1}(\boldsymbol{G} + s\boldsymbol{C})} \tag{3.3}$$

The existence and the expressions of these generators depend on the field coupling formulation adopted: they are both present in case of a "balanced" formulation [25], while the current source is absent in case of the "electric field" formulation [15], and the voltage source is omitted by the "magnetic filed" formulation [32]. The equivalent sources above are then used to augment the scattering parameters representation as follows

$$\begin{bmatrix} \boldsymbol{B}_1 \\ \boldsymbol{B}_2 \end{bmatrix} = \begin{bmatrix} \boldsymbol{S}_{11} & \boldsymbol{S}_{12} \\ \boldsymbol{S}_{21} & \boldsymbol{S}_{22} \end{bmatrix} \begin{bmatrix} \boldsymbol{A}_1 \\ \boldsymbol{A}_2 \end{bmatrix} + \begin{bmatrix} \overline{\boldsymbol{B}}_{f1} \\ \overline{\boldsymbol{B}}_{f2} \end{bmatrix} \tag{3.4}$$

The current wave variables are then converted into voltages and currents by the following transformation

$$\begin{aligned} \boldsymbol{I}_p &= \boldsymbol{Y}\boldsymbol{V}_p - 2\boldsymbol{B}_p \\ \boldsymbol{A}_p &= \boldsymbol{I}_p + \boldsymbol{B}_p \end{aligned} \tag{3.5}$$

where $p = 1, 2$ denote the near and far ends, respectively.

(3.4) and (3.5) can be used to provide an equivalent circuit representation in the form of the generalized Branin type. This developed equivalent circuit can be integrated easily in SPICE-like environments.

It should be noted here that the main derivations of the above formulation are obtained for uniform lines only. Another drawback with the above approach is that it does not address the issue of passivity.

3.2 Matrix Rational Approximation(MRA)

The Matrix Rational Approximation (MRA) approach was first proposed in [17] to address the issue of passivity. MRA is a closed-form approximation of the uniform transmission line and is based on the exponential matrix, and was extended in [33] to handle the problem of incident filed coupling. Using MRA enables writing the relation between the terminal voltages and currents in the following form.

$$\begin{bmatrix} \boldsymbol{V}(d,s) \\ \boldsymbol{I}(d,s) \end{bmatrix} = e^{\boldsymbol{Z}} \begin{bmatrix} \boldsymbol{V}(0,s) \\ \boldsymbol{I}(0,s) \end{bmatrix} + \begin{bmatrix} \boldsymbol{V}_F(d,s) \\ \boldsymbol{I}_F(d,s) \end{bmatrix} \tag{3.6}$$

where

$$\begin{aligned} \boldsymbol{Z} &= (\boldsymbol{D} + s\boldsymbol{E})d \\ \boldsymbol{D} &= \begin{bmatrix} \boldsymbol{0} & -\boldsymbol{R} \\ -\boldsymbol{G} & \boldsymbol{0} \end{bmatrix} \\ \boldsymbol{E} &= \begin{bmatrix} \boldsymbol{0} & -\boldsymbol{L} \\ -\boldsymbol{C} & \boldsymbol{0} \end{bmatrix} \end{aligned} \tag{3.7}$$

and d is the length of the line. $\boldsymbol{V}_F(d,s)$ and $\boldsymbol{I}_F(d,s)$ are the distributed sources representing the incident field. The matrix $e^{\boldsymbol{Z}}$ is approximated using matrix rational function as follows

$$e^{\boldsymbol{Z}} = \begin{bmatrix} \boldsymbol{T}_{11} & \boldsymbol{T}_{12} \\ \boldsymbol{T}_{21} & \boldsymbol{T}_{22} \end{bmatrix} \approx (\boldsymbol{P}_{N,M}(\boldsymbol{Z}))^{-1}\boldsymbol{Q}_{N,M}(\boldsymbol{Z}) \tag{3.8}$$

In (3.8), $\boldsymbol{T}$ is the state transition matrix. $\boldsymbol{P}_{N,M}(\boldsymbol{Z})$ and $\boldsymbol{Q}_{N,M}(\boldsymbol{Z})$ are given analytically in the form of predefined matrix polynomial, as shown next.

$$\begin{aligned} \boldsymbol{P}_{N,M}(\boldsymbol{Z}) &= \sum_{j=0}^{N} \frac{(M+N-j)!N!}{(M+N)!j!(N-j)!}(-\boldsymbol{Z})^j \\ \boldsymbol{Q}_{N,M}(\boldsymbol{Z}) &= \sum_{j=0}^{M} \frac{(M+N-j)!M!}{(M+N)!j!(M-j)!}(\boldsymbol{Z})^j \end{aligned} \tag{3.9}$$

In terms of admittance matrix (3.6) can be represented as

$$\begin{bmatrix} \boldsymbol{I}(0) \\ \boldsymbol{I}(d) \end{bmatrix} = \begin{bmatrix} -\boldsymbol{T}_{12}^{-1}\boldsymbol{T}_{11} & \boldsymbol{T}_{12}^{-1} \\ \boldsymbol{T}_{21} - \boldsymbol{T}_{22}\boldsymbol{T}_{12}^{-1}\boldsymbol{T}_{11} & \boldsymbol{T}_{22}\boldsymbol{T}_{12}^{-1} \end{bmatrix} \begin{bmatrix} \boldsymbol{V}(0) \\ \boldsymbol{V}(d) \end{bmatrix} + \begin{bmatrix} -\boldsymbol{T}_{12}^{-1} & \boldsymbol{0} \\ -\boldsymbol{T}_{22}\boldsymbol{T}_{12}^{-1} & \boldsymbol{U}_n \end{bmatrix} \begin{bmatrix} \boldsymbol{V}_F(d) \\ \boldsymbol{I}_F(d) \end{bmatrix} \tag{3.10}$$

The second term in the right hand of (3.10) represents the equivalent source at the end of line due to incident field coupling. The SPICE model for the equivalent source can be expressed in terms of rational functions.

3.3 Time Domain Space Expansion

Time Domain Space Expansion (TDSE) [30] method was developed to simulate the transient simulation of arbitrary Nonuniform Multiconductor Transmission Lines (NMTL) excited by external fields. The method is based on weak formulation obtained by expanding the voltages and currents along the line and the distributed sources due to the incident fields into some trial functions. Linear system of ODE's are obtained by taking the projection of the NMTL equations through suitable test functions. TDSE is used for lossless nonuniform transmission lines. The Telegrapher's equations for the case of lossless nonuniform transmission line excited by external electromagnetic field can be given by

$$\frac{d\boldsymbol{V}(z,t)}{dz} + \boldsymbol{L}(z)\frac{d\boldsymbol{I}(z,t)}{dz} = \boldsymbol{V}_F(z,t) \tag{3.11}$$

$$\frac{d\boldsymbol{I}(z,t)}{dz} + \boldsymbol{C}(z)\frac{d\boldsymbol{V}(z,t)}{dz} = \boldsymbol{I}_F(z,t) \tag{3.12}$$

For simplicity, the line is terminated by current controlled passive linear loads, which can be modeled with resistance matrices,

$$\boldsymbol{V}(0,t) = \boldsymbol{R}_S\boldsymbol{I}(0,t) \tag{3.13}$$

$$\boldsymbol{V}(1,t) = \boldsymbol{R}_L\boldsymbol{I}(1,t) \tag{3.14}$$

TDSE method adopts a trial function φ_n chosen so that only one is nonzero at each edge of the transmission line, namely φ_1 and φ_{N_φ}. The choice of the basis functions leads to the piecewise linear approximations of voltages, currents and per-unit length parameter matrices along the line. The voltage and currents along the line are approximated in therms of expansion coefficients into a set of trial functions φ_n.

$$\boldsymbol{V}(z,t) = \sum_{n=1}^{N_\varphi} \varphi_n(z)\boldsymbol{V}_n(t) \tag{3.15}$$

$$\boldsymbol{I}(z,t) = \sum_{n=1}^{N_\varphi} \varphi_n(z)\boldsymbol{I}_n(t) \tag{3.16}$$

Similarly the distributed voltage and current source due to the incident electromagnetic field is also approximated with the use of trial function.

$$\boldsymbol{V}_F(z,t) = \sum_{n=1}^{N_\varphi} \varphi_n(z)\boldsymbol{V}_{Fn}(t) \tag{3.17}$$

$$\boldsymbol{I}_F(z,t) = \sum_{n=1}^{N_\varphi} \varphi_n(z)\boldsymbol{I}_{Fn}(t) \tag{3.18}$$

Similarly the matrices formed by the per-unit length parameters L and C of MNTL are approximated with possibly different basis function φ_k.

$$\boldsymbol{L}(z) = \sum_{k=1}^{N_\varphi} \varphi_k(z)\boldsymbol{L}_k \tag{3.19}$$

$$\boldsymbol{C}(z) = \sum_{k=1}^{N_\varphi} \varphi_k(z)\boldsymbol{C}_k \tag{3.20}$$

Linear ODE's representing the spatial discretization of the original NMTL equations are obtained by projecting the equations onto a third set of functions η_m.

$$\sum_{n=1}^{N_\varphi} \boldsymbol{\Lambda}_{mn}\boldsymbol{V}_n(t) + \sum_{n=1}^{N_\varphi} \hat{\boldsymbol{L}}_{mn}\frac{d\boldsymbol{I}_n(t)}{dt} = \sum_{n=1}^{N_\varphi} \boldsymbol{E}_{mn}\boldsymbol{V}_{Fn}(t) \tag{3.21}$$

$$\sum_{n=1}^{N_\varphi} \boldsymbol{\Lambda}_{mn}I_n(t) + \sum_{n=1}^{N_\varphi} \hat{\boldsymbol{C}}_{mn}\frac{d\boldsymbol{V}_n(t)}{dt} = \sum_{n=1}^{N_\varphi} \boldsymbol{E}_{mn}\boldsymbol{I}_{Fn}(t) \tag{3.22}$$

where

$$\boldsymbol{\Lambda}_{mn} = \left\langle \frac{d\varphi_n}{dz}, \eta_m \right\rangle \boldsymbol{\mathcal{I}}_{\mathcal{P}} \tag{3.23}$$

$$\boldsymbol{E}_{mn} = \langle \varphi_n, \eta_m \rangle \boldsymbol{\mathcal{I}}_{\mathcal{P}} \tag{3.24}$$

$$\hat{\boldsymbol{L}}_{mn} = \sum_{k=1}^{N_\varphi} \boldsymbol{L}_k\boldsymbol{B}_{mn}^{(k)} \tag{3.25}$$

$$\hat{\boldsymbol{C}}_{mn} = \sum_{k=1}^{N_\varphi} \boldsymbol{L}_k\boldsymbol{B}_{mn}^{(k)} \tag{3.26}$$

where $\boldsymbol{\mathcal{I}}_{\mathcal{P}}$ is the $P \times P$ identity matrix and $\boldsymbol{B}_{mn}^{(k)} = \langle \varphi_n, \phi_k, \eta_m \rangle$, P represents the number of MNTL conductors. Since the trial functions are chosen such that only one is nonzero at

each edge therefore (3.13) and (3.14) translate into simple relations between the boarder voltage and current coefficients. The final ODE which is solved numerically by using 5^{th} and 6^{th} order Runge-Kutta scheme is

$$\psi \frac{d\boldsymbol{x}(t)}{dt} + \Phi x(t) = \Delta_F \boldsymbol{F}(t) \tag{3.27}$$

where ψ is nonsingular if the trial and test functions are linearly independent and Δ_F is a $P(2N_\varphi - 2) \times 2PN_\varphi$ highly sparse real matrix. The vector $\boldsymbol{x}$ collects the unknown expansion coefficients of voltage and current along the line while the vector $\boldsymbol{F}$ collects the expansion coefficients for the sources due to external fields.

TDSE method is implemented for lossless lines only. It is also observed that the method presupposed that the line to be terminated by the current controlled passive linear loads. Moreover the basis functions are chosen such that it lead to the piecewise linear approximations of voltages, currents, and per unit length parameter matrices along the line.

3.4 Model Decomposition Method

The commonly used method to solve the incident field coupling effect on nonuniform transmission lines is to solve the nonuniform transmission lines as cascade of uniform transmission lines. One of the methods developed [29] use a similar technique to solve the case of incident field coupling to nonuniform coupled microstrip transmission lines. In this technique, the nonuniform coupled microstrip transmission lines systems are first decomposed into a large number of uniform sections called steplines. Then modal decomposition method is used to model each step as a linear system with matrix coefficients. The external incident field are modeled as inputs in the proper positions of the system.

The total length of lines of system is divided into N uniform sections called steplines. Then the k^{th} strip at $x = x_k$ of the nth uniform step at $y_n < y < y_n + \Delta y$, where $y_n = (n-1)\Delta y$ is considered to obtain the voltage and current differential equations for Telegrapher's Equation for each step. The set of coupled differential equations for the n^{th} step lossless microstrip transmission lines is given by

$$\frac{d\boldsymbol{V}_n(y)}{dy} + jw\boldsymbol{L}_n\boldsymbol{I}_n(y) = \boldsymbol{v}_f(y) \tag{3.28}$$

$$\frac{d\boldsymbol{I}_n(y)}{dy} + jw\boldsymbol{C}_n\boldsymbol{V}_n(y) = \boldsymbol{i}_f(y) \tag{3.29}$$

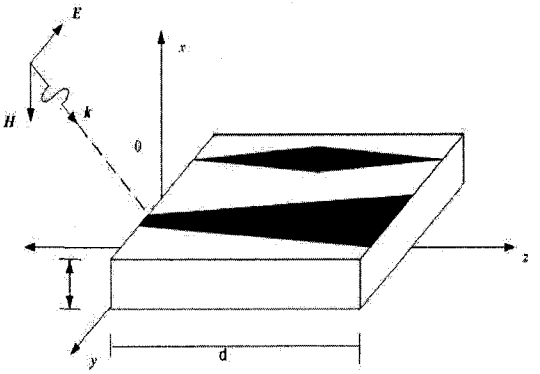

Figure 3.1: The system of externally excited nonuniform microstrip transmission lines

where $\boldsymbol{L}_n$ and $\boldsymbol{C}_n$ represents the per-unit length inductance and capacitance matrix, which are taken constant over the subinterval. $\boldsymbol{v}_f$ and $\boldsymbol{i}_f$ represent the equivalent voltage and current equation for the incident field coupling over the subinterval.

To solve the above coupled differential equations for $n = 1, 2 \ldots, N$, first they are decoupled by using the modal decomposition method introduced by [34]. The modal variables for the n^{th} step are defined by

$$\boldsymbol{V}_n^m(y) = \boldsymbol{T}_{vn}\boldsymbol{V}_n(y) \tag{3.30}$$

$$\boldsymbol{I}_n^m(y) = \boldsymbol{T}_{in}\boldsymbol{I}_n(y) \tag{3.31}$$

where $\boldsymbol{T}_{vn}$ and $\boldsymbol{T}_{in}$ are the frequency dependent transfer matrices for voltage and current for the n^th step. The uncoupled set of partial differential equations are obtained by substituting (3.30) and (3.31) into (3.28) and (3.29)

$$\frac{d\boldsymbol{V}_n^m(y)}{dy} + jw\boldsymbol{L}_n^m\boldsymbol{I}_n^m(y) = \boldsymbol{v}_f^m(y) \tag{3.32}$$

$$\frac{d\boldsymbol{I}_n^m(y)}{dy} + jw\boldsymbol{C}_n^m\boldsymbol{V}_n^m(y) = \boldsymbol{i}_f^m(y) \tag{3.33}$$

where $\boldsymbol{v}_f^m(y)$ and $\boldsymbol{i}_f^m(y)$ are the modal voltage and current sources due to distributed incident electromagnetic field and can be represented as

$$\boldsymbol{v}_{fn}^m(y) = \boldsymbol{T}_{vn}\boldsymbol{v}_{fn}(y) \tag{3.34}$$

$$i_{fn}^{m}(y) = \boldsymbol{T}_{in}\boldsymbol{i}_{fn}(y) \tag{3.35}$$

and

$$\boldsymbol{L}_{n}^{m} = \boldsymbol{T}_{vn}\boldsymbol{L}\boldsymbol{T}_{in}^{-1} \tag{3.36}$$

$$\boldsymbol{C}_{n}^{m} = \boldsymbol{T}_{in}\boldsymbol{C}\boldsymbol{T}_{vn}^{-1} \tag{3.37}$$

After applying the boundary conditions for both the input and the output terminals the induced terminal voltages is obtained as

$$\lambda \begin{bmatrix} \boldsymbol{V}_L \\ \boldsymbol{V}_S \end{bmatrix} = \xi \tag{3.38}$$

where

$$\lambda = \left[\begin{bmatrix} \boldsymbol{E}_{1N} & 0 \\ 0 & \boldsymbol{E}_{2N} \end{bmatrix}^{-1} \begin{bmatrix} [\boldsymbol{I}] \\ \boldsymbol{\Gamma}_L \end{bmatrix} \boldsymbol{M}_L^{-1} - \left(\prod_{n=N-1}^{1} \boldsymbol{S}_n \right) \begin{bmatrix} \boldsymbol{\Gamma}_g \\ [\boldsymbol{I}] \end{bmatrix} \boldsymbol{M}_g^{-1} \right] \tag{3.39}$$

and

$$\xi = \sum_{N-1}^{i=1} \left(\prod_{n=N-1}^{1} \boldsymbol{S}_n \right) \boldsymbol{X}_i + \left(\begin{bmatrix} \boldsymbol{E}_{1N} & 0 \\ 0 & \boldsymbol{E}_{2N} \end{bmatrix}^{-1} \begin{bmatrix} \boldsymbol{U}_N^{+} \\ \boldsymbol{U}_N^{-} \end{bmatrix} \right) \tag{3.40}$$

In this technique fullwave analysis is applied fist to analytically model the effect of an external electromagnetic field as a distributed voltage and current sources along the lines. This technique is used to solve for frequency domain analysis, while in the case of the time domain analysis there is no closed form solution and IFFT is used solve for that. Moreover since this technique used fullwave analysis its CPU intensive. Technique was applied for only lossless line. Moreover the technique is based on decomposing nonuniform transmission line into cascade of uniform transmission lines therefore the overall system size will be bigger and simulating this system would to solve this will be CPU intensive. Another difficulty with this approach is the spurious reflection due to the abrupt change in the characteristic impedance at the boundaries of each section of uniform transmission lines, which will further produce in accurate results.

3.5 Discussion

We have seen in the earlier sections that MOC and MRA algorithm can be applied for the case of uniform MTL. The basic assumption is the that current uniformly distributed throughout the cross section of the conductors, which is good for low operating frequency. As the operating frequency increases due to skin, edge and proximity effects [2] the current distribution get uneven and gets concentrated near the edge of the conductor. To model this effect, modeling based on frequency-dependent parameters may be necessary and hence matrices $\boldsymbol{R}$, $\boldsymbol{L}$, $\boldsymbol{G}$ and $\boldsymbol{C}$ will be function of frequency. It is difficult to get the time-domain PDEs [18] under this condition.

Simulation techniques discussed above to address the case of nonuniform transmission lines with incident field coupling have the basic approach of discritizing the nonuniform transmission line into cascade of many uniform transmission lines. When we descritize the nonuniform transmission line into cascade of uniform transmission line then we need large number of sections of uniform transmission line, which basically increase the system size and CPU cost to compute will increase and efficiency with decrease.

Chapter 4

Simulation of the Interconnect in the Presence of Incident Field

This chapter describes a new algorithm to simulate the electromagnetic field coupling with nonuniform Transmission Lines. The algorithm developed in this chapter can handle general nonuniform transmission lines with arbitrarily shaped PUL parameter matrices. The proposed algorithm can also be used to simulate the field coupling with uniform transmission lines as a special case.

The main idea behind the proposed technique is based on the concept of integrated congurance transform (ICT), which was first introduced in [35], [20] and later extended in [21] to simulate circuits with nonuniform TL's (NUMTL) but without incident electromagnetic fields. The work presented here seeks to generalize the concept of Integrated Congruence Transform, so that it can be used to simulate the effect of incident field on nonuniform transmission lines.

One of the basic advantages resulting from extending the concept of ICT to the problem of incident field coupling is the guarantee of passivity provided by the orthogonal projection technique used in the proposed algorithm. This fact represents a significant development since passivity-based algorithms available in the literature do not address the nonuniform transmission lines.

The work presented in this chapter assumes that the PUL parameter matrices of the line are given by a set of values at discrete points on the line and can be approximated using Chebyshev functions [36]. To facilitate illustrating the main ideas, the chapter starts by reviewing the application of ICT to simulate nonuniform transmission line in the absence of any incident electromagnetic field. This part is presented in section (4.1).

Using the ideas and terminology presented in this section, it will be possible to introduce the generalization to the case where incident electromagnetic field is present.

4.1 Integrated Congruence Transform

In this section we review the application of ICT to the simulation of circuits with nonuniform transmission lines under no incident electromagnetic field. To this end, we reproduce the Telegraphers's Equations in their homogeneous form, i.e., without the forcing term representing the incident field. We can write TEs as

$$\boldsymbol{T}\frac{\partial \boldsymbol{X}(z,s)}{\partial z} = -\left(\boldsymbol{N}(z) + s\boldsymbol{M}(z)\right)\boldsymbol{X}(z,s) \tag{4.1}$$

where

$$\begin{aligned} \boldsymbol{N}(z) &= \begin{bmatrix} \boldsymbol{R}(z) & \boldsymbol{0} \\ \boldsymbol{0} & \boldsymbol{G}(z) \end{bmatrix}, \quad \boldsymbol{M}(z) = \begin{bmatrix} \boldsymbol{L}(z) & \boldsymbol{0} \\ \boldsymbol{0} & \boldsymbol{C}(z) \end{bmatrix} \\ \boldsymbol{T} &= \begin{bmatrix} \boldsymbol{0} & \boldsymbol{I}_m \\ \boldsymbol{I}_m & \boldsymbol{0} \end{bmatrix}, \quad \boldsymbol{X}(z) = \begin{bmatrix} \boldsymbol{I}(z) \\ \boldsymbol{V}(z) \end{bmatrix} \end{aligned} \tag{4.2}$$

where $\boldsymbol{I}_m$ is an $m \times m$ identity matrix, $\boldsymbol{V}(z,s)$ and $\boldsymbol{I}(z,s)$ are the Laplace domain voltages and currents at an arbitrary point z along the transmission line, and m is the number of conductors.

The application of ICT in simulating the nonuniform transmission lines in a circuit simulation environment can be summed up as a two-phase process. In the first phase, reduced system matrices are first extracted by projecting the TE's into a Hilbert subspace. In the second phase, those reduced matrices are employed as a stamp to represent the NMTL as a circuit element within a general circuit, where circuit simulation techniques can be invoked to simulate the circuit behavior in the time or frequency-domain. A brief description of the above two phases is due next.

4.1.1 Phase-I: Extraction of NMTL stamp via projection

This step is best described by the schematic diagram sown in Figure 4.1 which depicts the main procedures in this phase in three conceptual stages. The basic computation in each stage is detailed next.

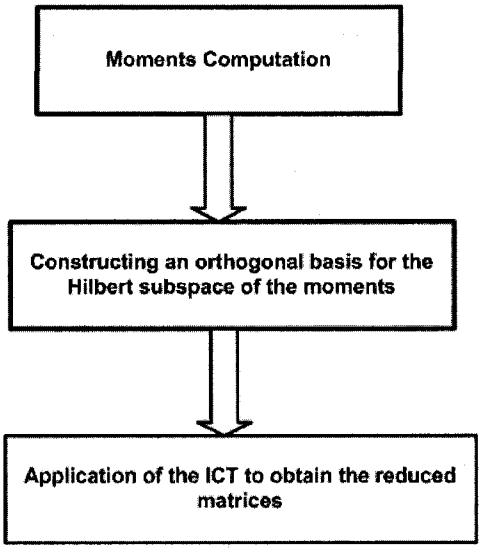

Figure 4.1: Pseudo-code to compute orthonormal basis spanning Hilbert space, first q moments

Moments Computation

The moments of TE's can be described precisely as follows. Denote by $\mathcal{X}(z,s)$ a set of $2m$ solutions for the TE's obtained under a set of $2m$ boundary conditions (BC), similar to those conditions that need to be specified if Y-parameters matrix of NTL is sought and the NTL is being treated as $2m$ – port network. Thus $\mathcal{X}(z,s)$ satisfies the following BCs

$$\mathcal{X}_V(0,s) = \begin{bmatrix} \boldsymbol{J}_m & \mathbf{0}_m \end{bmatrix} \tag{4.3}$$

$$\mathcal{X}_V(d,s) = \begin{bmatrix} \mathbf{0}_m & \boldsymbol{J}_m \end{bmatrix} \tag{4.4}$$

The subscript V in the above BC's is assigned to indicate that only the upper-half of $\mathcal{X}(z,s)$, the one corresponding to the voltage variables, is being considered, whereas a subscript I should indicate the lower half, the one that corresponds to the current variables. Also $\boldsymbol{J}_m$ and $\mathbf{0}_m$ are an $m \times m$ identity and zero matrices, respectively.

The moments of the TE's denoted by $\mathcal{U}^{(i)}(z,s_0)$, are defined as the Taylor series coefficients of $\mathcal{X}(z,s)$ when expanded at $s = s_0$, i.e.,

$$\mathcal{X}(z,s) = \sum_{i=0}^{\infty} \mathcal{U}^{(i)}(z,s_0)(s-s_0)^i \tag{4.5}$$

Computation of the moments is typically carried out by substituting from (4.5) into (4.2) and equating similar power of s. This leads to the following systems of differential equations

$$\boldsymbol{T}\frac{\partial \mathcal{U}^{(0)}(z)}{\partial z} = -(\boldsymbol{N}(z) + s_0\boldsymbol{M}(z))\mathcal{U}^{(0)}(z) \tag{4.6}$$

$$\boldsymbol{T}\frac{\partial \mathcal{U}^{(i)}(z)}{\partial z} = -(\boldsymbol{N}(z) + s_0\boldsymbol{M}(z))\mathcal{U}^{(i)}(z) - \boldsymbol{M}(z)\mathcal{U}^{(i-1)}(z) \tag{4.7}$$

The above system of equations are solved recursively as Boundary Value Problems (BVPs), where the BC's for $\mathcal{U}^{(i)}(z,s)$ are derived from the BCs in (4.3). In particular BC's for $\mathcal{U}^{(0)}(z,s)$ are obtained from

$$\mathcal{U}_V^{(0)}(0,s_0) = \begin{bmatrix} \boldsymbol{J}_m & \boldsymbol{0}_m \end{bmatrix} \tag{4.8}$$

$$\mathcal{U}_V^{(0)}(d,s_0) = \begin{bmatrix} \boldsymbol{0}_m & \boldsymbol{J}_m \end{bmatrix} \tag{4.9}$$

whereas BCs for $\mathcal{U}^{(i)}(z,s)$, $i > 0$ are obtained from

$$\mathcal{U}_V^{(i)}(0,s_0) = \begin{bmatrix} \boldsymbol{0}_m & \boldsymbol{0}_m \end{bmatrix} \tag{4.10}$$

$$\mathcal{U}_V^{(i)}(d,s_0) = \begin{bmatrix} \boldsymbol{0}_m & \boldsymbol{0}_m \end{bmatrix} \tag{4.11}$$

As described previously, a subscript V denotes the voltage portion of the moments.

Computing the lower half of the BC's of $\mathcal{U}^{(i)}(z,s_0)$, i.e., the one corresponding to the currents, $\mathcal{U}_I^{(i)}(z,s_0)$, is carried through the state transition matrix (STM). Let $\boldsymbol{\Phi}(z,s)$ denote the STM for the system of TE's then

$$\mathcal{U}^{(0)}(d,s_0) = \boldsymbol{\Phi}(d,s)\mathcal{U}^{(0)}(0,s_0) \tag{4.12}$$

$$\mathcal{U}^{(i)}(d,s_0) = \boldsymbol{\Phi}(d,s)\mathcal{U}^{(i)}(0,s_0) \tag{4.13}$$

We next partition $\boldsymbol{\Phi}(z,s)$ into 4 blocks as shown below

$$\mathbf{\Phi}(z,s) = \begin{bmatrix} \mathbf{\Phi}_{11} & \mathbf{\Phi}_{12} \\ \mathbf{\Phi}_{21} & \mathbf{\Phi}_{22} \end{bmatrix} \tag{4.14}$$

where each block is an $m \times m$ matrix, then substitute from (4.14), (4.8) and (4.9) into (4.12) to obtain

$$\mathcal{U}_I^{(0)}(0,s_0) = \begin{bmatrix} -\mathbf{\Phi}_{21}^{-1}(\mathbf{\Phi}_{22} \times \boldsymbol{J}_m) & \mathbf{\Phi}_{21}^{-1}(\boldsymbol{J}_m) \end{bmatrix} \tag{4.15}$$

Similar substitution from (4.14),(4.10) and (4.11) into (4.13) yields

$$\mathcal{U}_I^{(i)}(0,s_0) = \begin{bmatrix} \mathbf{0}_m & \mathbf{0}_m \end{bmatrix} \tag{4.16}$$

Notice here that both of (4.15) and (4.16) together with (4.8) and (4.10) represent a complete set of initial conditions IC's that respect the BC's specified previously and therefore enable solving both of (4.1) and (4.2) as IVP.

Computing the Orthonormal Basis

Once the system moments have been computed by solving (4.1) and (4.2) as explained above an orthonormal basis for their subspace can be constructed using the Modified-Gram Schmidth (MGS) [37]. However, given that these moments are functions of the spatial variable z, they can not be described properly as elements in a Classical Eucledian space, but rather should be treated as elements belonging to a generalized Hilbert Space which is denoted here as $\mathcal{L}(0,d)$. Using MGS to construct the orthogonal basis requires using the proper inner-product and norm mappings, which are defined as follows

$$(u(z)|v(z)) = \int_0^d u(z)^T v(z) dz \tag{4.17}$$

$$||u(z)|| = \int_0^d u(z)^T u(z) dz \tag{4.18}$$

where $u(z)$ and $u(z) \in \mathcal{L}(0,d)$.

Figure 4.1 depicts an algorithmic description for computing the orthonormal basis $\mathcal{Q}(z)$, that spans the Hilbert subspace of the first q moments, $\mathcal{U}^{(i)}(z,s)$, $0 \leq i \leq q$.

Algorithm 1: Hilbert Space Orth $(\mathcal{U}^{(i)}(z), q)$

INPUT: $(\mathcal{U}^{(i)}(z), q)$

/*The input argument is set of q elements, $\mathcal{U}^{(i)} \in \mathcal{L}(0,d)$, where $0 \leq i \leq q-1$. Each element is a matrix-shaped function of z with size $2m \times 2m$, where $0 \leq z \leq d$, and m is the number of conductors.*/

OUTPUT: An orthonormal basis $\mathcal{Q}(z)$ for the subspace of $\mathcal{U}^{(i)}(z)$.

;

;

/*Split the real and imaginary parts of the input arguments.*/

$\mathbf{S} \leftarrow \left\{\mathcal{R}\left\{\bigcup_{(i=0)}^{(q-1)} \mathcal{U}^{(i)}(z)\right\} \bigcup \xi\left\{\bigcup_{(i=0)}^{(q-1)} \mathcal{U}^{(i)}(z)\right\}\right\}$

/* Elements in (S) belong to $\mathcal{L}(0,d)$ and are vector-shaped functions of z with size $2m \times 1$.*/

$S \leftarrow |\mathbf{S}|$/* Number of elements in $\mathbf{S}$.*/

$\beta_0 \leftarrow ||\mathbf{S}_0(z)||$/ * Use (4.18) to compute the norm.*/

$\mathcal{Q}_{(0)}(z) \leftarrow \frac{1}{\beta_0}\mathbf{S}$

begin

  k=1

  while $k \leq$*S-1* **do**

    $\widetilde{\mathcal{Q}}_k(z) \leftarrow \mathcal{S}_{(k)}(z)$;

    h=0

    while $h \leq$*K-1* **do**

      $\widetilde{\mathcal{Q}}_k(z) \leftarrow \widetilde{\mathcal{Q}}_k(z) - \left\langle \widetilde{\mathcal{Q}}_k(z) | \widetilde{\mathcal{Q}}_h(z) \right\rangle \widetilde{\mathcal{Q}}_h(z)$ /*Use the definition of the inner-product in (4.17)

      $h = h + 1$

    $\beta_k \leftarrow \left\| \widetilde{\mathcal{Q}}_k(z) \right\|$;

    $\widetilde{\mathcal{Q}}_k(z) \leftarrow \frac{1}{\beta_k}\widetilde{\mathcal{Q}}_k(z)$

    $\mathcal{Q}(z) \leftarrow \left\{\bigcup_{i=0}^{L-1} \mathcal{Q}_i(z)\right\}$

    $k = k + 1$

end

Constructing the Reduced System Matrices

The reduced system matrices obtained at this stage represent the reduced-order model of the NMTL. The operations by which those matrices are obtained, starting from the TEs and with the help of $\mathcal{Q}(z)$, are described next.

To construct the reduced model, $\boldsymbol{X}(z,s)$ in (4.1) is replaced by another set of variables through the following change of variables

$$\boldsymbol{X}(z,s) \leftarrow \mathcal{Q}(z)\hat{\boldsymbol{X}}(s) \tag{4.19}$$

where matrix $\mathcal{Q}(z)$ is the orthonormal basis constructed earlier. Now substituting (4.19) into (4.1) premultiplying by $\mathcal{Q}^T(z)$ and integrating from 0 to d we obtain

$$(\hat{\boldsymbol{T}} + \hat{\boldsymbol{N}}_1 + s\hat{\boldsymbol{M}})\hat{\boldsymbol{X}}(s) = 0 \tag{4.20}$$

where,

$$\begin{aligned}
\hat{\boldsymbol{M}} &= \int_0^d \mathcal{Q}(z)^T \boldsymbol{M}(z)\mathcal{Q}(z)dz \\
\hat{\boldsymbol{N}}_1 &= \int_0^d \mathcal{Q}(z)^T \boldsymbol{N}(z)\mathcal{Q}(z)dz \\
\hat{\boldsymbol{T}} &= \int_0^d \mathcal{Q}(z)^T \boldsymbol{T}\frac{\mathcal{Q}(z)}{dz}dz
\end{aligned} \tag{4.21}$$

The transformation from (4.1) to (4.20) is called an integrated congruence transform w.r.t the transformation matrix $\mathcal{Q}(z)$. Now expanding the matrices $\hat{\boldsymbol{M}}$, $\hat{\boldsymbol{N}}_1$ and $\hat{\boldsymbol{T}}$ for computational purpose we get

$$\hat{\boldsymbol{M}} = \int_0^d (\mathcal{Q}_I^T(z)\boldsymbol{L}(z)\mathcal{Q}_I(z) + \mathcal{Q}_V^T(z)\boldsymbol{C}(z)\mathcal{Q}_V(z))dz \tag{4.22}$$

$$\hat{\boldsymbol{N}}_1 = \int_0^d (\mathcal{Q}_I^T(z)\boldsymbol{R}(z)\mathcal{Q}_I(z) + \mathcal{Q}_V^T(z)\boldsymbol{G}(z)\mathcal{Q}_V(z))dz \tag{4.23}$$

and

$$\hat{\boldsymbol{T}} = \int_0^d \left(\mathcal{Q}_I^T(z)\frac{d\mathcal{Q}_V(z)}{dz} + \mathcal{Q}_V^T(z)\frac{d\mathcal{Q}_I(z)}{dz}\right)dz \tag{4.24}$$

Splitting $\hat{\boldsymbol{T}}$ in two matrices such that $\hat{\boldsymbol{T}} = \hat{\boldsymbol{N}}_2 + \boldsymbol{P}$ where,

$$\boldsymbol{P} = \int_0^d \frac{d(\mathcal{Q}_I^T \mathcal{Q}_V(z))}{dz} dz = \mathcal{Q}_I^T(d)\mathcal{Q}_V(d) - \mathcal{Q}_I^T(0)\mathcal{Q}_V(0) \tag{4.25}$$

and $\hat{\boldsymbol{N}}_2$ by definition is given by

$$\hat{\boldsymbol{N}}_2 = \hat{\boldsymbol{T}} - \boldsymbol{P} \tag{4.26}$$

$$\begin{aligned} \hat{\boldsymbol{N}}_2 &= \int_0^d \left(\mathcal{Q}_I^T(z) \frac{d\mathcal{Q}_V(z)}{dz} + \mathcal{Q}_V^T(z) \frac{d\mathcal{Q}_I(z)}{dz} \right) dz - \int_0^d \frac{d(\mathcal{Q}_I^T \mathcal{Q}_V(z))}{dz} dz \\ &= \int_0^d \left(\mathcal{Q}_V^T(z) \frac{d\mathcal{Q}_I(z)}{dz} - \frac{d\mathcal{Q}_I^T(z)}{dz} \mathcal{Q}_V(z) \right) dz \end{aligned} \tag{4.27}$$

Note that

$$\hat{\boldsymbol{N}}_2^T = -\hat{\boldsymbol{N}}_2 \tag{4.28}$$

Defining

$$\hat{\boldsymbol{N}} = \hat{\boldsymbol{N}}_1 + \hat{\boldsymbol{N}}_2 \tag{4.29}$$

and using this definition in (4.20) to obtain

$$(s\hat{\boldsymbol{M}} + \hat{\boldsymbol{N}})\hat{\boldsymbol{X}}(s) = -\boldsymbol{P}\hat{\boldsymbol{X}}(s) \tag{4.30}$$

We also define the matrix $\hat{\boldsymbol{b}}$

$$\hat{\boldsymbol{b}} = \begin{bmatrix} \mathcal{Q}_I(0) \\ -\mathcal{Q}_I(d) \end{bmatrix}^T \tag{4.31}$$

The matrices $\hat{\boldsymbol{N}}$, $\hat{\boldsymbol{M}}$ and $\hat{\boldsymbol{b}}$ are the reduced system matrices used to represent the NMTL in a general circuit, as will be explained next.

4.1.2 Phase-II: Stamping the NMTL in a General Circuit

The matrices obtained from Phase-I are employed in this phase to represent the NMTL as a circuit element within a general circuit. For this purpose, we show how these matrices can be used to derive a relation between the terminal voltages and currents

$\boldsymbol{V}(0,s)$, $\boldsymbol{V}(d,s)$, $\boldsymbol{I}(0,s)$ and $\boldsymbol{I}(d,s)$. Such relation will serve as the constitutive equations needed to represent the NMTL as a circuit element. The voltages at the terminals of the transmission line network are obtained from

$$\boldsymbol{V}(s) = \begin{bmatrix} \boldsymbol{V}(0,s) \\ \boldsymbol{V}(d,s) \end{bmatrix} = \begin{bmatrix} \mathcal{Q}_V(0,s) \\ \mathcal{Q}_V(d,s) \end{bmatrix} \hat{\boldsymbol{X}}(s) \tag{4.32}$$

where subscript V in (4.32) denotes only that portion of the orthonormal basis corresponding to the voltage variables. From (4.25) matrix $\boldsymbol{P}$ can be defined as

$$\boldsymbol{P} = (\mathcal{Q}_I(d))^T \mathcal{Q}_V(d) - (\mathcal{Q}_I(0))^T \mathcal{Q}_V(0) \tag{4.33}$$

where subscript I in (4.33) denotes only that portion of $\mathcal{Q}(z)$ corresponding to the current variables. $\boldsymbol{V}(s)$ is can be obtained using

$$-\boldsymbol{P}\hat{\boldsymbol{X}}(s) = \hat{\boldsymbol{b}}\boldsymbol{V}(s) \tag{4.34}$$

Using $\mathcal{Q}(z)$ currents at the terminals of the network can be represented as

$$\boldsymbol{I}(s) = \begin{bmatrix} \mathcal{Q}_I(0) \\ -\mathcal{Q}_I(d) \end{bmatrix} \hat{\boldsymbol{X}}(s) = \hat{\boldsymbol{b}}^T \hat{\boldsymbol{X}}(s) \tag{4.35}$$

Using (4.34) in (4.30) and denoting the relation of (4.35) gives us the desired relation between the terminal voltages and currents in the following form

$$(\hat{\boldsymbol{N}} + s\hat{\boldsymbol{M}})\hat{\boldsymbol{X}}(s) = \hat{\boldsymbol{b}}\boldsymbol{V}(s) \tag{4.36}$$

$$\boldsymbol{I}(s) = \hat{\boldsymbol{b}}^T \hat{\boldsymbol{X}}(s) \tag{4.37}$$

The key advantage of he above constitutive relation for the NMTL is that it can be represented in the time-domain in the form of a set of ODE's. This fact enables representing the NMTL in general circuits with nonlinear elements. To illustrate this idea, we consider the circuit shown in Figure 4.2.

Using the reduced-order system constructed as described above, the circuit can be represented in the time domain using Modified Nodal Admittance [38](MNA) formulation as follows

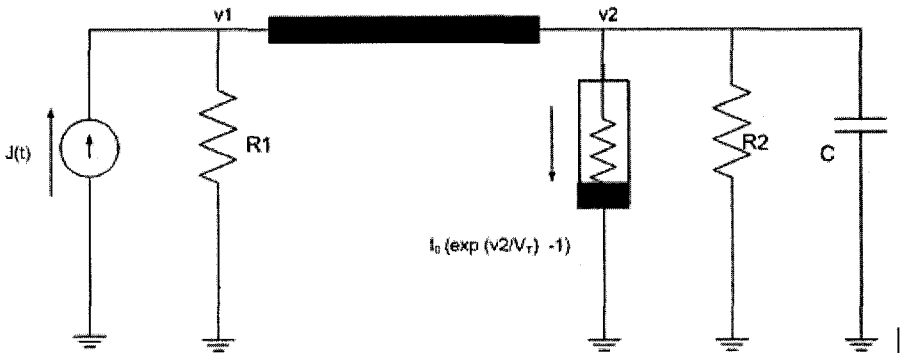

Figure 4.2: An example of a circuit containing a TL with nonlinear termination

$$\begin{bmatrix} \boldsymbol{G} & \boldsymbol{A}\hat{\boldsymbol{b}}^T \\ -\hat{\boldsymbol{b}}\boldsymbol{A}^T & \hat{\boldsymbol{N}} \end{bmatrix} \begin{bmatrix} v_1 \\ v_2 \\ \hat{\boldsymbol{x}}(t) \end{bmatrix} + \begin{bmatrix} \boldsymbol{C} & \boldsymbol{0} \\ \boldsymbol{0} & \hat{\boldsymbol{M}} \end{bmatrix} \begin{bmatrix} \frac{dv_1}{dt} \\ \frac{dv_2}{dt} \\ \frac{d\hat{\boldsymbol{x}}(t)}{dt} \end{bmatrix} + \begin{bmatrix} 0 \\ I_o\left(exp\left(v_2/V_T\right) - 1\right) \\ \boldsymbol{0} \end{bmatrix} = \begin{bmatrix} J(t) \\ 0 \\ \boldsymbol{0} \end{bmatrix} \tag{4.38}$$

where the matrices $\boldsymbol{G}$ and $\boldsymbol{C} \in \boldsymbol{R}^{2\times 2}$ are given by

$$\boldsymbol{G} = \begin{bmatrix} \frac{1}{R_1} & 0 \\ 0 & \frac{1}{R_2} \end{bmatrix}, \quad \boldsymbol{C} = \begin{bmatrix} C & 0 \\ 0 & 0 \end{bmatrix} \tag{4.39}$$

and $\hat{\boldsymbol{N}}$, $\hat{\boldsymbol{M}} \in \boldsymbol{R}^{2\times 2}$ are obtained using the proposed algorithm as shown above, with q being the size of the reduced system. $\boldsymbol{A}$ in (4.38) is an incidence matrix that maps the currents at the terminals of the TL to the nodes of the network. In the case of the above example, A is an 2×2 identity matrix.

4.2 Application of ICT to the EMI problems

In this section, the framework of the ICT described in the previous section is generalized so that it can handle NMTL's under incident electromagnetic field. For this purpose we consider the inhomogeneous TE's, where the incident field is used as the forcing term.

$$\boldsymbol{T}\frac{\partial \boldsymbol{X}_{\text{EMI}}(z,s)}{\partial z} = -\left(\boldsymbol{N}(z)+s\boldsymbol{M}(z)\right)\boldsymbol{X}_{\text{EMI}}(z,s)+E_0(s)\left(\boldsymbol{N}_F(z)+s\boldsymbol{M}_F(z)\right)\boldsymbol{V}_F(z)e^{-s\kappa_z z} \tag{4.40}$$

where,

$$\boldsymbol{N}_F(z) = \begin{bmatrix} \boldsymbol{G}(z) & \boldsymbol{0} \\ \boldsymbol{0} & \boldsymbol{0} \end{bmatrix} \tag{4.41}$$

$$\boldsymbol{M}_F(z) = \begin{bmatrix} \boldsymbol{C}(z) & \boldsymbol{0} \\ \boldsymbol{0} & \boldsymbol{J}_m \end{bmatrix} \tag{4.42}$$

$$\boldsymbol{V}_F(z) = \begin{bmatrix} \tilde{\boldsymbol{v}}_{F1} \\ \tilde{\boldsymbol{v}}_{F2} \end{bmatrix} \tag{4.43}$$

and $\boldsymbol{X}_{\text{EMI}}(z,s)$ represents the vector of distributed currents and voltages under the influence of the electromagnetic field.

Adopting the ICT framework to the EMI problem is carried out by modifying the procedural steps described in section (4.1) to take into account the presence of the forcing term in (4.40). Details of the required modifications to handle this situation are provided in the following subsections.

4.2.1 Phase-I: ICT-EMI

Similar to the schematic diagram depicted in Figure 4.1, this phase aims at constructing reduced matrices that can be used to abstract the NMTL as a system representing the line in a general circuit simulator environment.

ICT-EMI Moments Computations

The moments of the inhomogeneous TE are defined as the Taylor series coefficients of $\boldsymbol{X}_{\text{EMI}}(z,s)$, around some point s_0 in the Laplace-domain,

$$\boldsymbol{X}_{\text{EMI}}(z,s) = \sum_{i=0}^{\infty} \mathcal{U}_{\text{EMI}}^{(i)}(z,s_0)(s-s_0)^i \tag{4.44}$$

where, $\boldsymbol{X}_{\text{EMI}}(z,s)$ is a $2m \times 2m$ matrix in which the k^{th} column represent a solution to the in homogeneous TE, but with a BC corresponding to the k^{th} column of the Y-parameters matrix. Thus

$$\boldsymbol{X}_{\mathrm{EMI,V}}(0,s) = \left[\begin{array}{cc} \boldsymbol{J}_m & \boldsymbol{0}_m \end{array}\right] \tag{4.45}$$

$$\boldsymbol{X}_{\mathrm{EMI,V}}(d,s) = \left[\begin{array}{cc} \boldsymbol{0}_m & \boldsymbol{J}_m \end{array}\right] \tag{4.46}$$

To simplify the mathematical manipulations involved in computing the moments, we assume that $E(s)$ is equal to unity, that is the pulse waveform of the EM field is simply given by a unit impulse. Hence, substitution from (4.44) into (4.40) and equating similar powers of s gives the following system of differential equations.

$$\boldsymbol{T}\frac{\partial \mathcal{U}^{(0)}_{\mathrm{EMI}}(z,s_0)}{\partial z} = -\left(\boldsymbol{N}(z)+s_0\boldsymbol{M}(z)\right)\mathcal{U}^{(0)}_{\mathrm{EMI}}(z,s_0) + \left(\boldsymbol{N}_F(z)+s_0\boldsymbol{M}_F(z)\right)\boldsymbol{V}_F(z)e^{-s_0\kappa_z z} \tag{4.47}$$

$$\boldsymbol{T}\frac{\partial \mathcal{U}^{(i)}_{\mathrm{EMI}}(z,s_0)}{\partial z} = -\left(\boldsymbol{N}(z)+s_0\boldsymbol{M}(z)\right)\mathcal{U}^{(i)}_{\mathrm{EMI}}(z,s_0) - \boldsymbol{M}(z)\mathcal{U}^{(i-1)}_{\mathrm{EMI}} + (-\kappa_z z)^{i-1}\boldsymbol{M}_F(z)\boldsymbol{V}_F(z)e^{-s_0\kappa_z z} + (-\kappa_z z)^{i}\left(\boldsymbol{N}_F(z)+s_0\boldsymbol{M}_F(z)\right)\boldsymbol{V}_F(z)e^{-s_0\kappa_z z} \tag{4.48}$$

where $\mathcal{U}^{(0)}_{\mathrm{EMI},V}(0,s_0)$ is first found by solving (4.47) as a BVP, while higher order moments are computed by solving (4.48), recursively.

The BC's for $\mathcal{U}^{(i)}_{\mathrm{EMI},V}(z,s_0)$ are derived from the BC's of $\boldsymbol{X}_{\mathrm{EMI}}(z,s)$ and are specified as follows

$$\mathcal{U}^{(0)}_{\mathrm{EMI},V}(0,s_0) = \left[\begin{array}{cc} \boldsymbol{J}_m & \boldsymbol{0}_m \end{array}\right] \tag{4.49}$$

$$\mathcal{U}^{(0)}_{\mathrm{EMI},V}(d,s_0) = \left[\begin{array}{cc} \boldsymbol{0}_m & \boldsymbol{J}_m \end{array}\right] \tag{4.50}$$

$$\mathcal{U}^{(i)}_{\mathrm{EMI},V}(0,s_0) = \mathcal{U}^{(i)}_{\mathrm{EMI},V}(d,s_0) = \left[\begin{array}{cc} \boldsymbol{0}_m & \boldsymbol{0}_m \end{array}\right] \tag{4.51}$$

where a subscript V means, as before, that the lower portion of $\mathcal{U}^{(i)}_{\mathrm{EMI},V}(z,s_0)$ is considered in the assignment. To obtain the BC's of the upper portion, i.e., the one corresponding

to the currents, we employ the notion of the STM described before,

$$\begin{bmatrix} \mathcal{U}^{(0)}_{\mathrm{EMI},I}(d,s_0) \\ \mathcal{U}^{(0)}_{\mathrm{EMI},V}(d,s_0) \end{bmatrix} = \begin{bmatrix} \mathbf{\Phi}_{11} & \mathbf{\Phi}_{21} \\ \mathbf{\Phi}_{21} & \mathbf{\Phi}_{22} \end{bmatrix} \begin{bmatrix} \mathcal{U}^{(0)}_{\mathrm{EMI},I}(0,s_0) \\ \mathcal{U}^{(0)}_{\mathrm{EMI},V}(0,s_0) \end{bmatrix} + \mathcal{H}^{(0)}_F(d,s_0) \tag{4.52}$$

for $i = 0$, and

$$\begin{bmatrix} \mathcal{U}^{(i)}_{\mathrm{EMI},I}(d,s_0) \\ \mathcal{U}^{(i)}_{\mathrm{EMI},V}(d,s_0) \end{bmatrix} = \begin{bmatrix} \mathbf{\Phi}_{11} & \mathbf{\Phi}_{21} \\ \mathbf{\Phi}_{21} & \mathbf{\Phi}_{22} \end{bmatrix} \begin{bmatrix} \mathcal{U}^{(i)}_{\mathrm{EMI},I}(0,s_0) \\ \mathcal{U}^{(i)}_{\mathrm{EMI},V}(0,s_0) \end{bmatrix} + \mathcal{H}^{(i)}_F(d,s_0) \tag{4.53}$$

for $i > 0$, where

$$\mathcal{H}^{(0)}_F(d,s_0) = \int_0^d \mathbf{\Phi}(\tau,s_0)\left(\boldsymbol{N}_F(\tau) + s_0\boldsymbol{M}_F(\tau)\right)\boldsymbol{V}_F(\tau)e^{-s_0\kappa_z\tau}\mathrm{d}\tau \tag{4.54}$$

$$\begin{aligned}\mathcal{H}^{(i)}_F(d,s_0) = &-\int_0^d \mathbf{\Phi}(\tau,s_0)\boldsymbol{M}(\tau)\mathcal{U}^{(i-1)}_{\mathrm{EMI}}(\tau)\mathrm{d}\tau \\ &+\int_0^d \mathbf{\Phi}(\tau,s_0)(-\kappa_z\tau)^{i-1}\boldsymbol{M}_F(\tau)\boldsymbol{V}_F(\tau)e^{-s_0\kappa_z\tau}\mathrm{d}\tau \\ &+\int_0^d \mathbf{\Phi}(\tau,s_0)(-\kappa_z\tau)^{i}\left(\boldsymbol{N}_F(\tau) + s_0\boldsymbol{M}_F(\tau)\right)\boldsymbol{V}_F(\tau)e^{-s_0\kappa_z\tau}\mathrm{d}\tau\end{aligned} \tag{4.55}$$

Partitioning $\mathcal{H}^{(i)}_F(d,s_0)$ as shown below

$$\mathcal{H}^{(i)}_F(d,s_0) := \begin{bmatrix} \boldsymbol{H}^{(i)}_{11} & \boldsymbol{H}^{(i)}_{12} \\ \boldsymbol{H}^{(i)}_{21} & \boldsymbol{H}^{(i)}_{22} \end{bmatrix} \tag{4.56}$$

and substitution from the BC's for $\mathcal{U}^{(i)}_{\mathrm{EMI},V}(0,s_0)$, we obtain the initial conditions for $\mathcal{U}^{(0)}_{\mathrm{EMI},I}(0,s_0)$ as follows

$$\begin{bmatrix} \mathbf{0}_m & \boldsymbol{J}_m \end{bmatrix} = \begin{bmatrix} \mathbf{\Phi}_{21} & \mathbf{\Phi}_{22} \end{bmatrix}\left[\mathcal{U}^{(0)}_{\mathrm{EMI}}(0,s_0)\right] + \begin{bmatrix} \boldsymbol{H}^{(0)}_{21} & \boldsymbol{H}^{(0)}_{22} \end{bmatrix} \tag{4.57}$$

$$\begin{bmatrix} \mathbf{0}_m & \mathbf{0}_m \end{bmatrix} = \begin{bmatrix} \mathbf{\Phi}_{21} & \mathbf{\Phi}_{22} \end{bmatrix}\left[\mathcal{U}^{(i)}_{\mathrm{EMI}}(0,s_0)\right] + \begin{bmatrix} \boldsymbol{H}^{(i)}_{21} & \boldsymbol{H}^{(i)}_{22} \end{bmatrix} \tag{4.58}$$

Solving (4.57) and (4.58) enables finding a complete set of initial conditions that

satisfy the BC's given earlier.

$$\mathcal{U}^{(i)}_{\text{EMI}}(0,s_0) = \begin{bmatrix} \mathcal{U}^{(i)}_{\text{EMI},I}(0,s_0) \\ \mathcal{U}^{(i)}_{\text{EMI},V}(0,s_0) \end{bmatrix} \tag{4.59}$$

Using the above initial conditions, the solutions to the BVP's of the moments can be constructed back again

$$\mathcal{U}^{(i)}_{\text{EMI}}(z,s_0) = \underbrace{\boldsymbol{\Phi}(z,s_0)\mathcal{U}^{(i)}_{\text{EMI}}(0,s_0)}_{\text{homogenuous solution}} + \underbrace{\mathcal{H}^{(i)}(z,s_0)}_{\text{particular solution}} \tag{4.60}$$

Notice that the particular solution portion represents the solution to the inhomogeneous TE under zero initial conditions. Further details on how to compute the STM $\boldsymbol{\Phi}(z,s_0)$ and the particular solution will be provided in section (4.3).

Computation of the Orthonormal Basis

Once the moments have been computed as shown above, construction of an orthonormal basis spanning their Hilbert subspace can proceed as explained earlier for the case where there is no EMI. We denote the orthonormal basis in this case by $\mathcal{Q}_{\text{EMI}}(z)$.

Computation of the Reduced System

Constructing the reduced matrices representing the system of the NMTL under EMI proceeds in a similar manner to constructing the reduced matrices when there was no EMI, but with an additional modifications to take into consideration the presence of the forcing term in the TE's that represents the incident fields. First a change of variables is performed in (4.40), whereby $\boldsymbol{X}_{\text{EMI}}(z,s)$ is replaced by $\mathcal{Q}_{\text{EMI}}(z)\hat{\boldsymbol{X}}(s)$ and then the system of (4.40) is pre-multiplied by $\mathcal{Q}_{\text{EMI}}(z)^T$, and integrated from $0,d$, on both sides. This yields the following system

$$\left(\hat{\boldsymbol{T}} + \hat{\boldsymbol{N}}_1 + s\hat{\boldsymbol{M}}\right)\hat{\boldsymbol{X}}(s) = \hat{\boldsymbol{U}}_F(s) \tag{4.61}$$

where

$$\hat{\boldsymbol{U}}_F(s) = E_0(s)\int_0^d \mathcal{Q}_{\text{EMI}}(z)^T\left(\boldsymbol{N}_F(z) + s\boldsymbol{M}_F(z)\right)\boldsymbol{V}_F(z)e^{-s\kappa_z z}\mathrm{d}z \tag{4.62}$$

while $\hat{\boldsymbol{N}}$, $\hat{\boldsymbol{M}}$ and $\hat{\boldsymbol{T}}$ are given as before in (4.21) but with $\mathcal{Q}(z)$ replaced by $\mathcal{Q}_{\text{EMI}}(z)$. One can proceed with mathematical manipulations similar to those carried out earlier

to show that (4.61) can be used to deduce a relation between the terminal currents and terminal voltages as follows

$$\begin{aligned}\left(\hat{\boldsymbol{N}}+s\hat{\boldsymbol{M}}\right)\hat{\boldsymbol{X}}(s) &= \hat{\boldsymbol{b}}\boldsymbol{V}(s)+\hat{\boldsymbol{U}}_F(s)\\ \boldsymbol{I}(s) &= \hat{\boldsymbol{b}}^T\hat{\boldsymbol{X}}(s)\end{aligned} \tag{4.63}$$

where $\hat{\boldsymbol{N}}$, $\hat{\boldsymbol{M}}$ and $\hat{\boldsymbol{T}}$ are given as before in (4.21) but with $\mathcal{Q}(z)$ replaced by $\mathcal{Q}_{\text{EMI}}(z)$.

4.2.2 Phase-II: ICT-EMI

The reduced system obtained in (4.63) can be used to represent the NMTL under EMI as a simple circuit element within a general circuit. For example, consider the circuit shown earlier in Figure (4.2) and, assume that the circuit is exposed to electromagnetic field. A generalized formulation of the circuit equations, which include the effect of the electromagnetic field on the transmission line can be written as follows.

$$\left\{\begin{bmatrix}\boldsymbol{G} & \boldsymbol{A}\hat{\boldsymbol{b}}^T\\ -\hat{\boldsymbol{b}}\boldsymbol{A}^T & \hat{\boldsymbol{N}}\end{bmatrix}\begin{bmatrix}v_1\\ v_2\\ \hat{\boldsymbol{x}}(t)\end{bmatrix}+\begin{bmatrix}\boldsymbol{C} & \boldsymbol{0}\\ \boldsymbol{0} & \hat{\boldsymbol{M}}\end{bmatrix}\begin{bmatrix}\frac{dv_1}{dt}\\ \frac{dv_2}{dt}\\ \frac{d\hat{\boldsymbol{x}}(t)}{dt}\end{bmatrix}\right\}$$
$$+\begin{bmatrix}0\\ I_o\left(exp\left(v_2/V_T\right)-1\right)\\ \boldsymbol{0}\end{bmatrix}=\begin{bmatrix}J(t)\\ 0\\ \hat{\boldsymbol{u}}_F(t)\end{bmatrix} \tag{4.64}$$

where the matrices $\boldsymbol{G}$ and $\boldsymbol{C}\in\boldsymbol{R}^{2\times 2}$ are given by

$$\boldsymbol{G}=\begin{bmatrix}\frac{1}{R_1} & 0\\ 0 & \frac{1}{R_2}\end{bmatrix},\quad \boldsymbol{C}=\begin{bmatrix}C & 0\\ 0 & 0\end{bmatrix} \tag{4.65}$$

In (4.64) $\hat{\boldsymbol{u}}_F(t)$ is the inverse Laplace transform of $\hat{\boldsymbol{U}}_F(s)$.

4.3 Further Computational Details

In this section, we present further computational details related to the computation of the STM, $\boldsymbol{\Phi}(z,s_0)$ and the particular solution of the BVP (4.47) and (4.48). The presentation of this section is carried out in an analogous manner to the derivation presented in [21]. We first start by describing computation of $\boldsymbol{\Phi}(z,s_0)$.

4.3.1 Computing STM $\boldsymbol{\Phi}(z, s_0)$

Given that the STM, $\boldsymbol{\Phi}(z, s_0)$, is the matrix-valued solution of the homogeneous differential equations, i.e., the solution obtained in the absence of any forcing terms, with an IC given by a unity matrix of the same size [39], then considering (4.7), $\boldsymbol{\Phi}(z, s_0)$ becomes the solution of the following system

$$\left(\boldsymbol{T}\frac{d}{dz} + \boldsymbol{N}(z) + s_0\boldsymbol{M}(z)\right)\boldsymbol{\Phi}(z,0) = \boldsymbol{J}_{2\mathrm{m}}\delta(z) \tag{4.66}$$

We can express $\boldsymbol{\Phi}(z,0)$ in Chebyshev series with $H+1$ polynomials,

$$\boldsymbol{\Phi}(z,0) = \sum_{h=0}^{H} \boldsymbol{\Xi}_{\boldsymbol{\Phi},h} T_h(\overline{z}) \tag{4.67}$$

Using the identities

$$\begin{aligned}
T_m(\overline{z})T_n(\overline{z}) &= \frac{1}{2}(T_{m+n}(\overline{z}) + T_{|m-n|}(\overline{z})) \\
\int_{-1}^{\overline{z}} T_0(\xi)d\xi &= T_0(\overline{z}) + T_1(\overline{z}) \\
\int_{-1}^{\overline{z}} T_1(\xi)d\xi &= \frac{1}{4}(T_2(\overline{z}) - T_0(\overline{z})) \\
\int_{-1}^{\overline{z}} T_h(\xi)d\xi &= \frac{1}{2}\left(\frac{T_{h+1}(\overline{z})}{h+1} + \frac{T_{h-1}(\overline{z})}{h-1}\right)\frac{(-1)^{h+1}}{h^2-1}
\end{aligned} \tag{4.68}$$

in (4.66) and integrating yields, the following linear system in the coefficients $\boldsymbol{\Xi}_{\boldsymbol{\Phi},h}$,

$$\left[\mathcal{A} + \frac{2}{d}\left(\boldsymbol{J}_{H+1} \otimes \boldsymbol{T}\right)\right]\tilde{\boldsymbol{\Lambda}}_{\boldsymbol{\Phi}} = \boldsymbol{\Upsilon}_0 \tag{4.69}$$

The operator $\otimes$ is the Kronecker product. In (4.69),

$$\mathcal{A} = \frac{1}{2}\left(\mathcal{T}_1 + \mathcal{T}_2 + \mathcal{T}_3\right) \tag{4.70}$$

and

$$\tilde{\boldsymbol{\Lambda}}_{\boldsymbol{\Phi}} = \left[\boldsymbol{\Xi}^T_{\boldsymbol{\Phi},H} \;\; \boldsymbol{\Xi}^T_{\boldsymbol{\Phi},H-1} \;\cdots\; \boldsymbol{\Xi}^T_{\boldsymbol{\Phi},0}\right] \tag{4.71}$$

and

$$\Upsilon_0 = \left[\underbrace{\mathbf{0}\ \mathbf{0}\cdots\mathbf{0}}_{H \text{ matrices}}\ \ \boldsymbol{J}_{2\mathrm{m}}\right]^T \tag{4.72}$$

In (4.70) matrices $\mathcal{T}_1$, $\mathcal{T}_2$ and $\mathcal{T}_3$ are defined as

$$\mathcal{T}_1 = \begin{bmatrix} 0 & \cdots & 0 & \frac{1}{2H}D_H & \frac{1}{2H}D_{H-1} \\ 0 & \cdots & \frac{1}{2H-1}D_H & \frac{1}{2H-1}D_{H-1} & \frac{1}{2H-1}(D_{H-2}-D_H) \\ \vdots & \ddots & \vdots & \vdots & \vdots \\ \vdots & \ddots & D_2-\frac{1}{2}D_4 & D_1-\frac{1}{2}D_3 & D_0-\frac{1}{2}D_2 \\ D_H & \cdots & \cdots & \begin{pmatrix} D_1-\frac{1}{4}D_2+ \\ \sum_{h=2}^{H-1} D_h\frac{(-1)^h+1}{h^2-1} \end{pmatrix} & \begin{pmatrix} D_0-\frac{1}{4}D_1+ \\ \sum_{h=2}^{H} D_h\frac{(-1)^h+1}{h^2-1} \end{pmatrix} \end{bmatrix} \tag{4.73}$$

$$\mathcal{T}_2 = \begin{bmatrix} \frac{1}{2H}D_1 & 0 & \cdots & \cdots & 0 & 0 \\ \frac{1}{2H-1}(D_2-D_0) & \frac{1}{2H-1}D_1 & 0 & \cdots & 0 & 0 \\ \vdots & \cdots & \cdots & \ddots & \vdots & \vdots \\ \frac{1}{4}(D_{H-1}-D_{H-3}) & \cdots & \frac{1}{4}D_1 & \frac{1}{4}D_0 & 0 & 0 \\ -\frac{1}{2}D_{H-2} & \cdots & -\frac{1}{2}D_1 & -\frac{1}{2}D_0 & 0 & 0 \\ \begin{pmatrix} -\frac{1}{4}D_{H-1}+ \\ \sum_{h=2}^{H} D_{H-h}\frac{(-1)^h+1}{h^2-1} \end{pmatrix} & \cdots & \cdots & -\frac{1}{4}D_1-\frac{1}{3}D_0 & -\frac{1}{4}D_0 & 0 \end{bmatrix} \tag{4.74}$$

$$\mathcal{T}_3 = \begin{bmatrix} 0 & \cdots & \cdots & \frac{1}{2H}(D_{H-2}-D_H) & \frac{1}{2H}D_{H-1} \\ 0 & \ddots & \ddots & \cdots & \vdots \\ \vdots & -\frac{1}{4}D_0 & -\frac{1}{4}D_1 & \frac{1}{4}(D_0-D_2) & \frac{1}{4}(D_0-D_2) \\ 0 & 0 & -\frac{1}{2}D_0 & -\frac{1}{2}D_1 & D_0-\frac{1}{2}D_2 \\ D_0 & \cdots & \sum_{h=2}^{H} D_{h-2}\frac{(-1)^h+1}{h^2-1} & \begin{pmatrix} -\frac{1}{4}D_0+ \\ \sum_{h=2}^{H} D_{h-1}\frac{(-1)^h+1}{h^2-1} \end{pmatrix} & \begin{pmatrix} D_0-\frac{1}{4}D_1+ \\ \sum_{h=2}^{H} D_h\frac{(-1)^h+1}{h^2-1} \end{pmatrix} \end{bmatrix} \tag{4.75}$$

4.3.2 Computing The Particular Solution

This computation is carried out on the same basis used above to compute $\mathbf{\Phi}(z, s_0)$. In this part, the differential equations are assigned Zero Initial Conditions, and the forcing term is expressed using Chebyshev expansion, where by integration we obtain a linear system in the Chebyshev coefficients of the particular solution. Once, the particular solution has been obtained in Chebyshev form, it can be added to the Chebyshev coefficients of the STM multiplied by the desired initial conditions. This constitutes the complete solution to the BVP according to the desired BC's.

Chapter 5

Numerical Examples

Special examples of TLs, for which an exact solution of TEs in the frequency-domain can be obtained analytically, have been considered for validating the results obtained from the proposed algorithm. Exact solutions in the frequency-domain are obtained by adjusting BCs of analytical TEs solutions according to the TL terminations with the external circuitry. Time-domain responses are then approximated via applying the Inverse Fast Fourier Transform (IFFT) on data sampled from the frequency-domain solutions. In all of the those experiments, the incident field is assumed to have a piecewise-linear-shaped pulse launched at $t = 3$ ns, with a rise/fall time of 0.1 ns and a pulse-width of 1.9 ns. Also the incidence angles of the fields are assumed to be $\theta = 60°$, $\phi = -90°$, whereas the polarization angle of the electric field is given by $\theta_E = -90°$ [2], and the amplitude of the pulse is 0.2 kV/m. The reduced system is constructed by matching the first two derivatives at points ($s = 1, 3, 5, 7, 9 \times j2\pi \times 10^9$ Hz).

5.1 Example 1: A Uniform MTL

The first example considered is a uniform MTL (length = 10cm) with three conductors and a ground plane. The physical structure of the TL, its PUL parameter matrices and circuit terminations have been described in [19]. For a UMTL, the exact solution can always be constructed analytically using the exponential matrix [40], while the incident field excitations can be represented by well-known equivalent terminal sources [2]. Figures 5.1 - 5.6 shows the time-domain waveforms at the terminals of the three conductors obtained using the proposed algorithm and compares them with the waveforms obtained from IFFT.

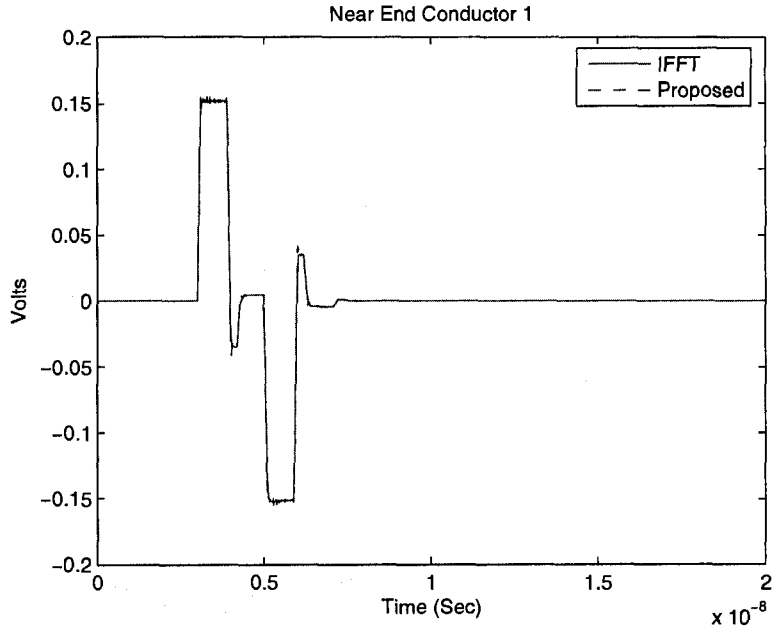

Figure 5.1: Time-domain waveform at near end of conductor-1 for TL used in Example 1.

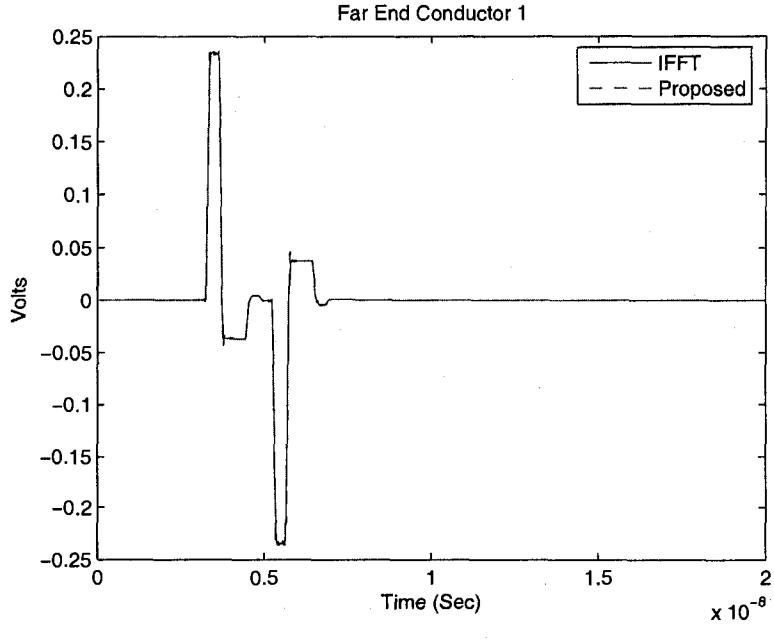

Figure 5.2: Time-domain waveform at far end of conductor-1 for TL used in Example 1.

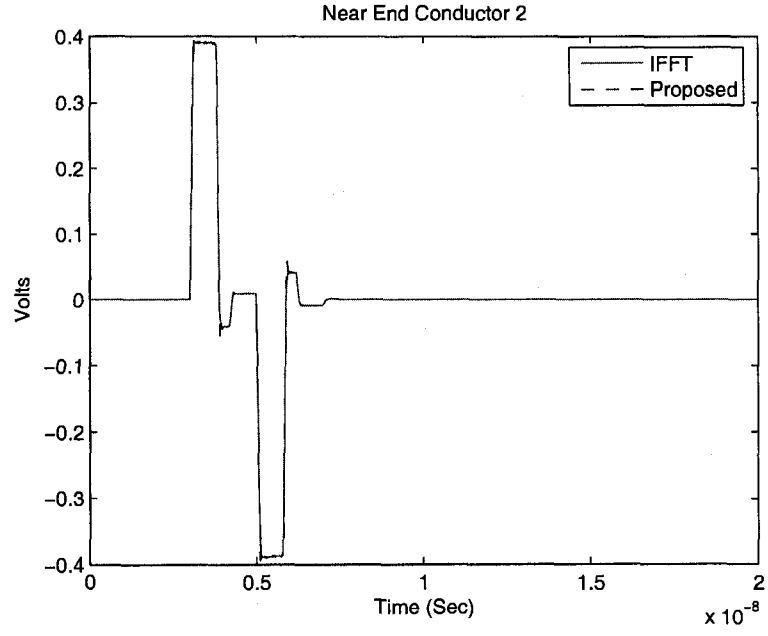

Figure 5.3: Time-domain waveform at near end of conductor-2 for TL used in Example 1.

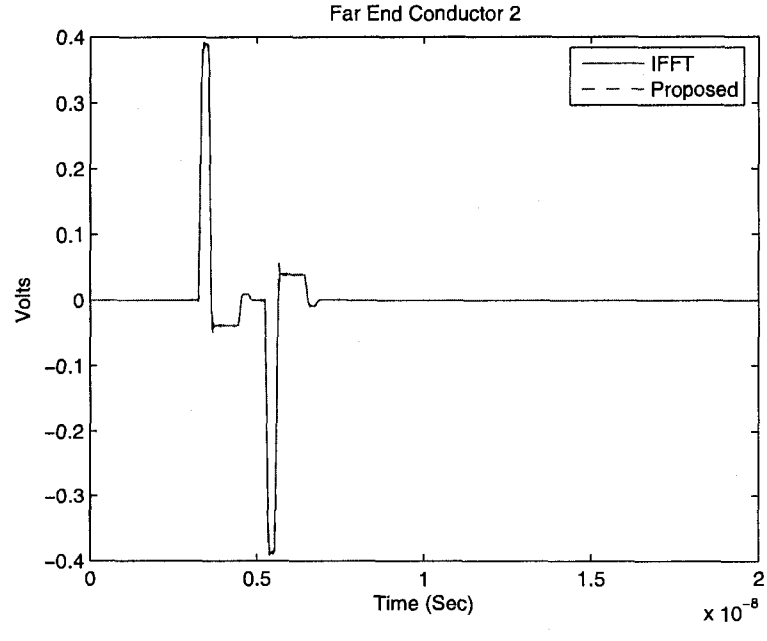

Figure 5.4: Time-domain waveform at far end of conductor-2 for TL used in Example 1.

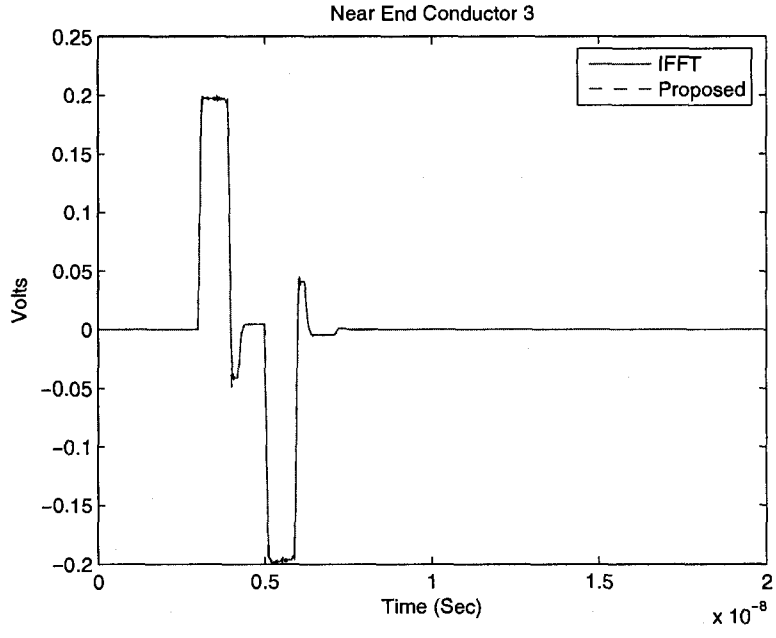

Figure 5.5: Time-domain waveform at near end of conductor-3 for TL used in Example 1.

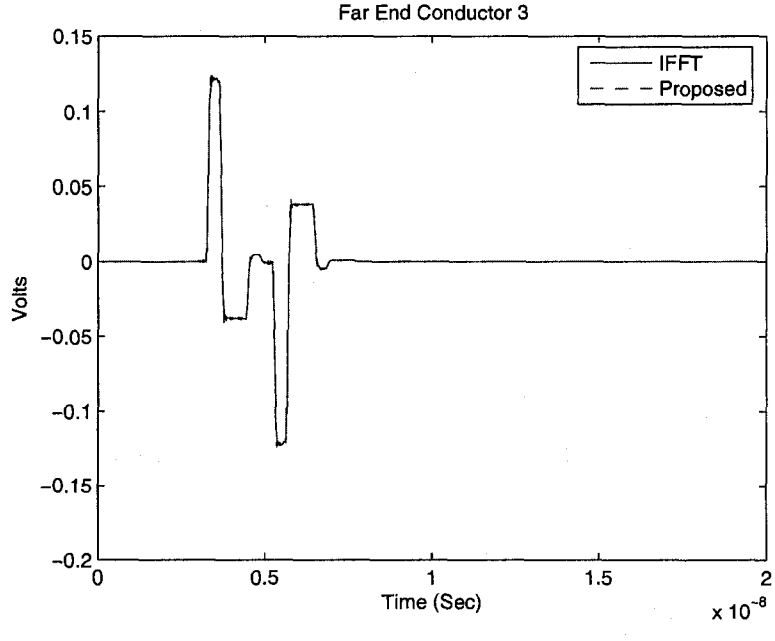

Figure 5.6: Time-domain waveform at far end of conductor-3 for TL used in Example 1.

5.2 Example 2: A Tapered Single-Conductor Nonuniform TL

The exponentially tapered lossless TL with one conductor and a ground reference plane ($m = 1$) is a special case of NMTLs for which an analytical solution for the TE in the frequency-domain can be found a-priori [41]. The PUL parameters for this TL are given by, $L(z) = L_0 e^{\delta z}$, $C(z) = C_0 e^{-\delta z}$ with $L_0 = \mu_0 \epsilon_0 (1/C_0)$, where $\delta = 10 \ln 4 \, \mathrm{m}^{-1}$, $0 \leq z \leq 0.1\mathrm{m}$, and $C_0 = 100p\mathrm{F/m}$. The TL was driven by an input pulse, V_s, having a rise/fall time of 0.1 ns with pulse width 7.9 ns launched at $t = 1$ ns, under two cases of terminations described by the schematic diagrams of Fig. 5.7 and Fig. 5.8. Figures 5.9 - 5.12 shows the responses computed by the proposed algorithm in the two cases of terminations and compares them with IFFT results.

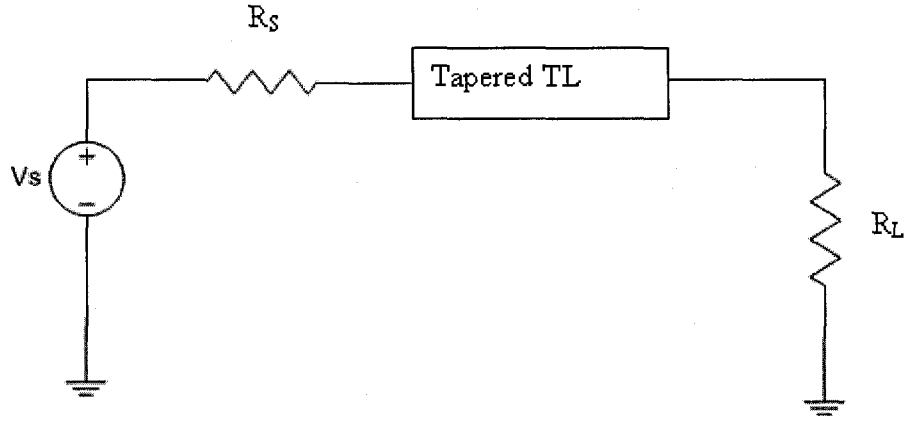

Figure 5.7: Case I: Terminations given by $R_S = 31\Omega, R_L = 126\Omega$

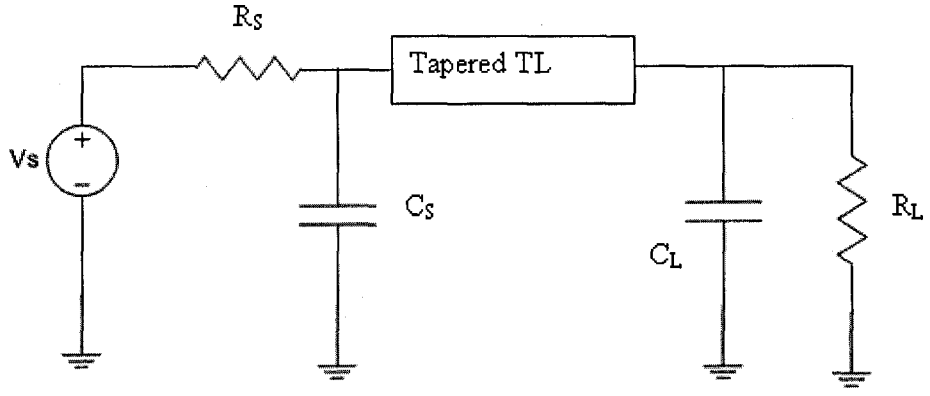

Figure 5.8: Case II: Terminations given by $R_S = 31\Omega, R_L = 126\Omega, C_S = 1\text{pF}, C_L = 0.4\text{pF}$

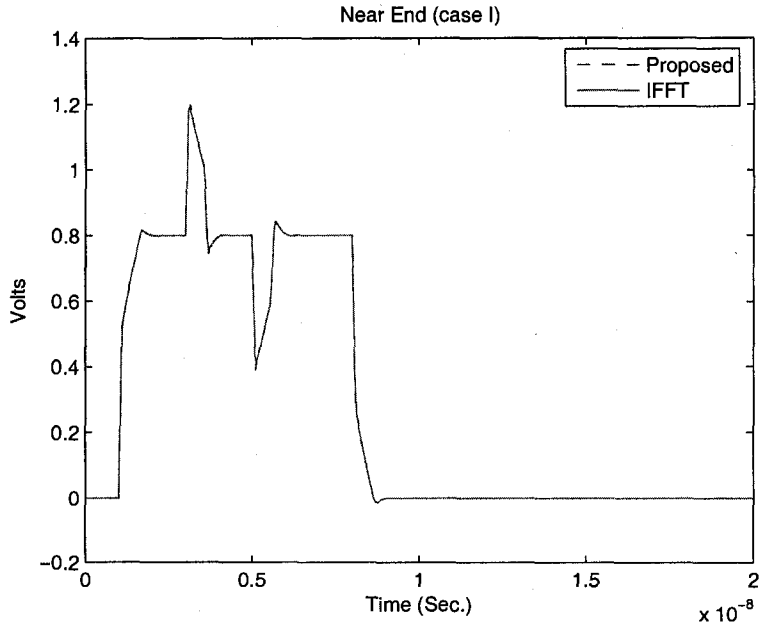

Figure 5.9: Time-domain response at near end of conductor for Case I.

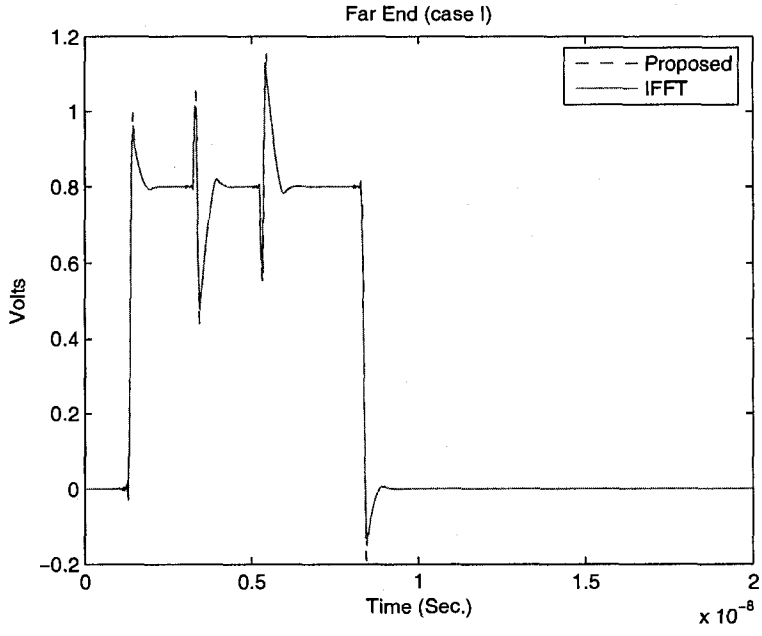

Figure 5.10: Time-domain response at far end of conductor for Case I.

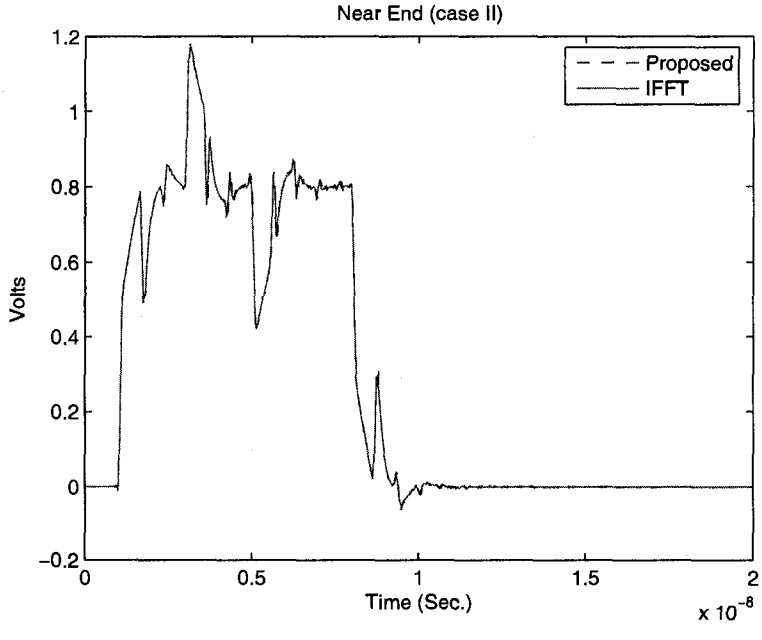

Figure 5.11: Time-domain response at near end of conductor for Case II.

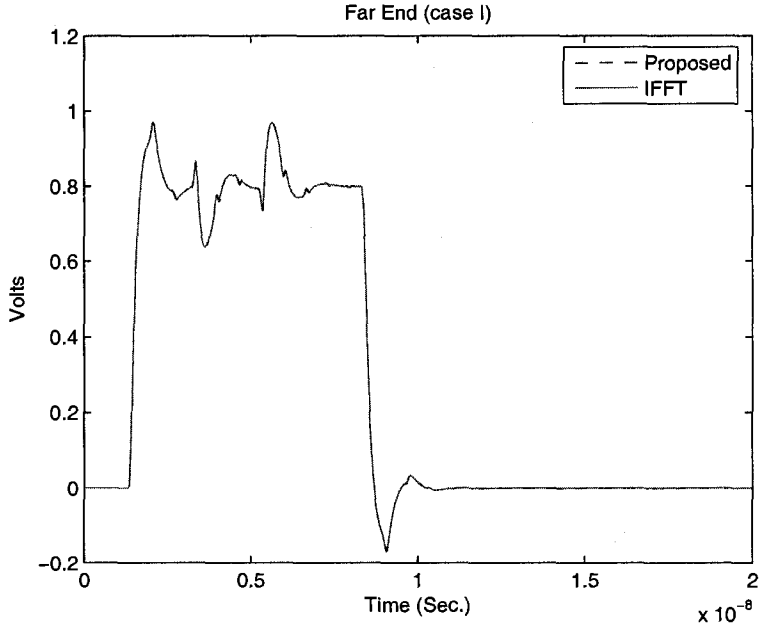

Figure 5.12: Time-domain response at far end of conductor for Case II.

Chapter 6

Conclusion and Future Work

This chapter contains a summary of the work that was presented in this thesis. In addition, directions for future work are also discussed.

6.1 Summary

In this thesis, ICT algorithm was efficiently extended for the case of nonuniform transmission line exposed to electromagnetic field. The thesis proposed the macromodel using ICT for the nonuniform transmission line and equivalent source due to incident field coupling that is suitable for the circuit simulators. The major advantages of the proposed algorithm are as follows.

1. The proposed macromodel reduced the order of the system while preserved the passivity of the macromodel. The passivity of the macromodel is guaranteed by construction.

2. The proposed algorithm was also used to simulate the case of multiconductor uniform transmission lines and single conductor tapered non-uniform transmission line excited by incident electromagnetic field.

6.2 Future Work

The following further research directions are proposed

1. Sensitivity Analysis: The algorithm in this thesis provides the closed form characterization of the influence of external electromagnetic fields. Therefore, they can be used for sensitivity analysis of the NMT networks to EMI [42].

2. Time Domain Solution: In the present algorithm once we get the frequency domain solution we use IFFT techniques to get the time domain solution. Further work is required to get the closed form solution in case of time domain solution.

3. Inhomogeneous medium effects: The various simulation techniques proposed to simulate the incident field coupling on interconnects have treated the medium surrounding the interconnects as homogeneous. However the effect due to inhomogeneous medium is very significant and could be subject of further investigation [43].

4. Nonuniform incident fields: The proposed work approximate the distant radiating source as a uniform plane wave incident field. However interference on transmission lines due to nearby sources can no longer be treated as as plane waves. To account for nearby sources, the proposed algorithm will have to consider other forms of forcing terms in the Telegraphers equations which could impact the way the reduced system is constructed.

Bibliography

[1] R. Achar and M. Nakhla, "Simulation of high-speed interconnects," *Proc. of the IEEE*, vol. 89, pp. 693–728, May 2001.

[2] C. Paul, *Analysis of Multiconductor Transmission Lines.* John Wiley & Sons, Inc, 1994.

[3] I.Erdin, A. Dounavis, R. Achar, and M. Nakhla, "A spice model for incident field coupling to multiconductor transmission lines," *IEEE Transactions on Electromagnetic Compatibility*, vol. 43, no. 4, pp. 449–461, Nov 2001.

[4] G.Shinh, N. Nakhla, R. Achar, M. Nakhla, A. Dounavis, and I. Erdin, "Efficient spice macromodel for emi analysis of electronic packages and high speed interconnects," in *IEEE Electrical Performance of Eletronic Packaging (EPEP)*, Oct. 2004, pp. 277–280.

[5] R. Khazaka and M. Nakhla, "Analysis of high-speed interconnects in the presence of electromagnetic interference," *IEEE Trans. Microw. Theory Tech*, vol. 46, no. 7, pp. 940–947, July 1998.

[6] E. Chiprout and M. Nakhla, "Analysis of interconnect networks using complex frequency hopping (chf)," *IEEE Transactions on Computer-Aided Design*, pp. 186–200, Feb 1995.

[7] L. Pillage and R. Rohrer, "Asymptotic waveform evaluation for timing analysis," *IEEE Transactions on Computer-Aided Design*, vol. 9, pp. 352–366, Apr 1990.

[8] Y.Kami and R. Sato, "Circuit-concept approach to externally exited transmission lines," *IEEE Trans. on EMC*, vol. 27, no. 4, pp. 177–183, Nov 1985.

[9] C. R. Paul, "Literal solutions for the time-domain response of a two-wire transmission line excited by an incident electromagnetic field," *IEEE Trans. Electromagnetic Compat.*, vol. 37, no. 2, pp. 241–251, May 1995.

[10] ——, "A spice model for multiconductor transmission lines excited by an incident electromagnetic field," *IEEE Trans. Electromagnetic Compat.*, vol. 36, no. 4, pp. 342–354, Nov 1994.

[11] F. B. Jr., "Transient analysis of lossless transmission lines," *Proceeding of IEEE*, vol. 55, pp. 2012–2013, 1967.

[12] N. Orthanovic, P. Wang, and V. Tripathi, "Generalized method of characteristics for time-domain simulation of multiconductor lossy transmission lines," *IEEE International Symposium on Circuit and Systems*, pp. 2388–2391, May 1990.

[13] R. K. Das and W. Smith, "Incident field coupling analysis of multiconductor transmission lines using asymptotic waveform evaluation," in *In Proc. IEEE Int. Symp. Electromagnetic Compt.*, Aug. 1996, pp. 265–270.

[14] T. Tang, M. Nakhla, and R. Griffith, "Analysis of lossy multiconductor transmission lines using the asymptotic waveform evaluation techniques," *IEEE Trans. Microw. Theory Tech.*, vol. 39, no. 12, pp. 2107–2116, Dec 1991.

[15] A. Agrawal, H. Price, and S. Gurbaxani, "Transient response of a multiconductor transmission lines excited by a nonuniform electromagnetic field," *IEEE Trans. on Electromagnetic Compatibility*, vol. 22, pp. 119–129, May 1980.

[16] I. Maio, F. canavero, and B. Dilecce, "Analysis of crosstalk and field coupling to lossy mtl's in a spice environment," *IEEE Transactions on Electromagnetic Compatbility*, vol. 38, no. 3, pp. 221–229, Aug. 1996.

[17] A. Dounaivs, X. Li, M. Nakhla, and R. Achar, "Passive closed-form transmission line model for general purpose circuit simulators," *IEEE Transactions on Microwave Theory and Techniques*, vol. 47, pp. 2450–2459, Dec. 1999.

[18] A. Dounavis, R. Achar, and M. Nakhla, "A general class of passvie macromodels for lossy multiconductor transmission lines," *IEEE Trans. Mcirowave Theory Tech.*, vol. 49, pp. 1686–1696, Oct. 2001.

[19] G. S. Shinh, N. M. Nakhla, R. Achar, M. S. Nakhla, and A. Dounavis, "Fast transient analysis of incident field coupling to multiconductor transmission lines," *IEEE Trans. on Electromagnetic Compt.*, vol. 48, no. 1, pp. 57–73, Feb. 2006.

[20] Q.Yu, J.M.L.Wang, and E. Kuh, "Passive multipoint moment matching model order reduction algorithim of multiport distributed interconnect networkds," *IEEE Trans. on Circuits and Systems*, vol. 46, no. 1, pp. 140–160, Jan. 1999.

[21] E. Gad and M. Nakhla, "Efficient simulation of nonunifrom transmission lines using integrated congruence transform," *IEEE Trans. Very Large Scale Integration*, vol. 12, pp. 1307–1320, Dec. 2004.

[22] Y.-C. Lu, M. Celik, T. Young, and L. T. Pileggi, "Min/max on-chip inductance models and delay metrics," in *IEEE Proc. of the 38th Conference on Design Automation*, 2001, pp. 341 – 346.

[23] R. Khazaka, "High-speed interconnect analysis in the presence of incident elctromagnetic fields," Master's thesis, Carleton University, Dec. 1997.

[24] A. Smith, "A more convenient form of the equations for the response of a transmission line excited by nonuniform fields," *IEEE Trans. on EMC*, vol. 15, pp. 151–152, Aug 1973.

[25] C. Taylor, R. Satterwhite, and C. Harrison, "The response of a terminated two-wire transmission line excited by a nonuniform electromangetic field," *IEEE Trans. on Antennas Propagation*, vol. 13, pp. 987–989, Nov. 1965.

[26] C. Paul, *Analysis of Multiconductor Transmission Lines.* John Wiely & Sons Inc., 1994, ch. 7, pp. 395–422.

[27] C. Balanis, *Advanced Engineering Electromagnetics*, suruz, Ed. John Wiley & Sons, 1989.

[28] C. Paul and S. Nasar, *Introduction to Electromagetic Fields*, McGraw-Hill, Ed. McGraw-Hill, 1987.

[29] A. Cheldavi, "Field coupling to nonuniform coupled microstrip transmission lines," *International Journal of RF and Microwave Computer Aided-Engineering*, vol. 13, no. 3, pp. 215–228, March 2003.

[30] S. Grivet-Talocia and F. G. Canavero, "A transient solution for nonuniform multiconductor transmission lines in external fields," in *3th International Symposium on Electromagnetic Compatibility, Zurich (Switzerland)*, Feb. 16-18 1999, pp. 451–456.

[31] I. Maio and F. Canavero, "Transient field coupling and crosstalk in lossy lines with arbitrary loads," *IEEE Transactions on Electromagnetic Compatibility*, vol. 37, no. 6, pp. 599–606, Nov. 1995.

[32] F. Rachidi, "Formulation of field to transmission line coupling equations in terms of magnetic excitation field," *IEEE Trans. Electromag. Compat.*, vol. 35, pp. 404–407, Aug 1993.

[33] M. I. Elfadel, A. Dounavis, H. Huang, M. S. Nakhla, A. E. Ruehli, and R. Achar, "Accuracy and performance of passive transmission line macromodels based on optimal matrix rational approximations," in *Electrical Performance of Electronic Packaging*, 2002.

[34] G.-T. Lei, G.-W. Pan, and B. Gilbert, "Examination, clarification and simplification of modal decoupling method for multiconductor transmission lines," *IEEE Trans. Microwave Theory Tech*, vol. 43, no. 9, pp. 2090–2099, Sept. 1995.

[35] Y. Qingjian, J. M. Wang, and E. Kuh, "Multipoint moment matching model reduction for multiport distributed interconnect networks," in *IEEE ACM Int. Conference on Computer-Aided Design*, Nov. 1998, pp. 85–91.

[36] T. J. Rivlin, *Chebyshev polynomials*, N. Y. J. Wiley, Ed. J. Wiley, 1990.

[37] G. Golub and C. V. Loan, *Matrix Computation*, J. H. Press, Ed. Johns Hopkins Press, 1989.

[38] C. Ho, A. Ruehli, and P. Brennan, "The modified nodal approach to network analysis," *IEEE Trans. Circuits Syst.*, vol. 22, pp. 504–509, June 1975.

[39] H. D'Angelo, *Linear Time-Varying Systems: Analysis and Synthesis*, Allyn and Bacon, Eds. Allyn and Bacon, Boston, 1970.

[40] A. Dounavis, X. Li, M. S. Nakhla, and R. Achar, "Passive closed-form transmission line model for general purpose circuit simulators," *IEEE Trans. on Microwave Theory and Tech.*, vol. 47, no. 12, pp. 2450–2459, Dec. 1999.

[41] S. Grivet-Talocia and F. Canavero, *Interconnects in VLSI Design.* Kluwer, 2000, ch. 1.

[42] E. Gad and M. Nakhla, "Simulation and sensitivity analysis of nonuniform transmission lines using integrated congurence transform," *IEEE Trans. on Advance Packaging*, vol. 28, pp. 32–44, Feb. 2005.

[43] W. Bandurski and A. Dobrzaski, "Simulation of the coupling of the external electromagnetic field to pcb traces in the spice simulator," *International Journal of RF and Microwave Computer-Aided Engineering*, vol. 14, no. 2, pp. 190–200, March 2004.